G-CSF maintains controlled neutrophil mobilization during acute inflammation by negatively regulating CXCR2 signaling

Besnik Bajrami,[1,2,3]* Haiyan Zhu,[4]* Hyun-Jeong Kwak,[1,2,3] Subhanjan Mondal,[1,2,3] Qingming Hou,[1,2,3] Guangfeng Geng,[4] Kutay Karatepe,[1,2,3] Yu C. Zhang,[1,2,3] César Nombela-Arrieta,[1,2,3,5] Shin-Young Park,[1,2,3] Fabien Loison,[1,2,3] Jiro Sakai,[1,2,3] Yuanfu Xu,[4] Leslie E. Silberstein,[1,2,3] and Hongbo R. Luo[1,2,3]

[1]Department of Pathology, Harvard Medical School, Boston, MA 02115
[2]Department of Lab Medicine, The Stem Cell Program, Joint Program in Transfusion Medicine, Children's Hospital Boston, Boston, MA 02115
[3]Dana-Farber/Harvard Cancer Center, Boston, MA 02115
[4]The State Key Laboratory of Experimental Hematology, Institute of Hematology and Blood Diseases Hospital, Center for Stem Cell Medicine, Chinese Academy of Medical Sciences and Peking Union Medical College, Tianjin 300020, China
[5]Department of Experimental Hematology, University Hospital Zurich, 8091 Zurich, Switzerland

Cytokine-induced neutrophil mobilization from the bone marrow to circulation is a critical event in acute inflammation, but how it is accurately controlled remains poorly understood. In this study, we report that CXCR2 ligands are responsible for rapid neutrophil mobilization during early-stage acute inflammation. Nevertheless, although serum CXCR2 ligand concentrations increased during inflammation, neutrophil mobilization slowed after an initial acute fast phase, suggesting a suppression of neutrophil response to CXCR2 ligands after the acute phase. We demonstrate that granulocyte colony–stimulating factor (G-CSF), usually considered a prototypical neutrophil-mobilizing cytokine, was expressed later in the acute inflammatory response and unexpectedly impeded CXCR2-induced neutrophil mobilization by negatively regulating CXCR2-mediated intracellular signaling. Blocking G-CSF in vivo paradoxically elevated peripheral blood neutrophil counts in mice injected intraperitoneally with *Escherichia coli* and sequestered large numbers of neutrophils in the lungs, leading to sterile pulmonary inflammation. In a lipopolysaccharide-induced acute lung injury model, the homeostatic imbalance caused by G-CSF blockade enhanced neutrophil accumulation, edema, and inflammation in the lungs and ultimately led to significant lung damage. Thus, physiologically produced G-CSF not only acts as a neutrophil mobilizer at the relatively late stage of acute inflammation, but also prevents exaggerated neutrophil mobilization and the associated inflammation-induced tissue damage during early-phase infection and inflammation.

INTRODUCTION

Neutrophils are major players in innate immunity. They are recruited from circulation to infected tissues in response to infection, where they phagocytose and clear invading bacterial and fungal pathogens. However, excessive accumulation or hyperactivation of neutrophils can also be detrimental to the host. Hence, neutrophil homeostasis, recruitment, and function need exquisite regulation (Christopher and Link, 2007; von Vietinghoff and Ley, 2008; Strydom and

Rankin, 2013; Bardoel et al., 2014; Nauseef and Borregaard, 2014; Kruger et al., 2015).

Leukocytes, including neutrophils, arise from self-renewing hematopoietic stem cells that produce differentiated lineage-committed progenitors. Granulocyte/macrophage progenitors produce neutrophils via a series of developmental stages: first as myoblast, promyelocytes, myelocytes, metamyelocytes (at which point cell division ceases), and band neutrophils and then mature segmented neutrophils (Kondo et al., 2003). Neutrophils remain in the BM for 5–6 d after the last granulocyte precursor division, and consequently, the BM is the main site of neutrophil reserves. During acute infection and inflammation, large numbers of neutrophils are recruited to affected tissues, and mature neutrophils are mobilized from

---

The Rockefeller University Press $30.00
J. Exp. Med. 2016 Vol. 213 No. 10   1999–2018
www.jem.org/cgi/doi/10.1084/jem.20160393

1999

the BM to peripheral blood (PB) to compensate for their peripheral loss. This transient neutrophilia ensures that neutrophils are rapidly delivered to sites of infection.

The regulation of neutrophil and progenitor cell mobilization during acute inflammation has been extensively studied (Furze and Rankin, 2008; Sadik et al., 2011; Day and Link, 2012). Granulocyte CSF (G-CSF) is a prototypical neutrophil-mobilizing cytokine under both basal and stress conditions (Petit et al., 2002; Semerad et al., 2002; Broxmeyer, 2008; Knudsen et al., 2011; Dale, 2012; Bendall and Bradstock, 2014). After a single G-CSF injection, PB neutrophil numbers increase significantly, peak at 6 h, and return to near-baseline levels by 24 h (Lévesque et al., 2003; Semerad et al., 2005; Kim et al., 2006; De La Luz Sierra et al., 2007). G-CSF is also a hematopoietic cytokine and has multiple functions in normal, steady-state hematopoiesis including the regulation of neutrophil progenitor proliferation and differentiation and the functional activation of neutrophils (Gregory et al., 2007). Several other neutrophil-mobilizing agents are thought to contribute to stress-induced mobilization, the most notable being C5a, leukotriene B4 (LTB4), and CXCR2 ligands (e.g., IL-8 in humans and keratinocyte chemoattractant [KC] and macrophage inflammatory protein 2 [MIP-2] in mice; Martin et al., 2003; Burdon et al., 2005; Eash et al., 2010). CXCR2 ligand–induced neutrophil mobilization is much quicker than G-CSF–induced mobilization, with 10-fold neutrophilia occurring 30 min after injection (Fibbe et al., 1999). The rapidity of CXCR2-induced mobilization (minutes to hours) compared with G-CSF (hours to days) suggests that there are distinct mobilization mechanisms. Similar effects have also been seen in G-CSF– and CXCR2 ligand–induced mobilization of hematopoietic stem/progenitor cells (Pelus and Fukuda, 2006).

Here, we report that rapid neutrophil mobilization at the early stages of acute inflammation is mainly mediated by CXCR2 ligands. Although serum CXCR2 ligand concentrations increased during inflammation, neutrophil mobilization slowed after an initial acute fast phase. This suggests that neutrophil responses to CXCR2 ligands are suppressed after the acute phase: we demonstrate that this is caused by the inhibition of CXCR2-mediated cellular signaling by G-CSF, which was expressed later in the acute inflammatory response. Although G-CSF is a well known neutrophil-mobilizing agent, inhibition of G-CSF activity in vivo unexpectedly elevated PB neutrophil counts in *Escherichia coli*–infected mice and, furthermore, sequestered neutrophils in the lungs to produce sterile pulmonary inflammation. Similarly, in an LPS-induced acute lung injury model, G-CSF blockade led to enhanced neutrophil accumulation in the lungs, edema, and severe lung inflammation. Thus, G-CSF not only acts as a neutrophil mobilizer, but also negatively regulates neutrophil mobilization by CXCR2 ligands: this is a previously unrecognized neutrophil mobilization control mechanism during infection and inflammation. Furthermore, we demonstrate that the homeostatic imbalance caused by G-CSF suppression

elicits neutrophil sequestration in the lungs and ultimately leads to significant lung damage.

RESULTS

The instant PB neutrophilia induced by *E. coli* is mediated by CXCR2 ligands

To investigate the mechanism by which neutrophils are rapidly mobilized by chemokines and cytokines, we used a mouse peritonitis model of acute inflammation. Neutrophil numbers in the PB were elevated shortly after i.p. *E. coli* administration, with maximum blood levels reached at 90 min (Fig. 1 A). The majority of the increase occurred in the first 30 min after induction of peritoneal infection, suggesting that the regulatory cytokines must have similar dynamics (Fig. 1 B). Cytokine-specific ELISAs showed that levels of the CXCR2 ligands MIP-2 (Fig. 1 C) and KC (Fig. 1 D) rapidly increased in blood serum, peaking at 30 min after *E. coli* injection. CXCR2 ligands appeared to be essential for neutrophil mobilization at this early phase of acute infection, as simultaneous injection of CXCR2-blocking antibodies suppressed *E. coli*–induced neutrophilia (Fig. 1 E). Treatment with CXCR2 ligand alone was also sufficient to induce PB neutrophilia. The effect of MIP-2 on neutrophil mobilization was monitored by i.v. injection of MIP-2. 15 min after a single MIP-2 injection, there was a significant increase in circulating neutrophil numbers that was completely inhibited by CXCR2 antibodies (Fig. 1 F). Collectively, early neutrophil mobilization from the BM to the PB in response to acute infection appears to be caused, at least in part, by elevation of CXCR2 ligands in the blood.

G-CSF suppresses early-phase PB neutrophilia induced by *E. coli*

G-CSF is involved in the differentiation of myeloid progenitor cells into neutrophils and is also routinely used to mobilize neutrophils from the BM in neutropenic patients. We examined the effect of G-CSF on *E. coli*–induced neutrophilia at different time points. Surprisingly, G-CSF did not further increase neutrophil numbers in the PB of *E. coli*–challenged mice; on the contrary, G-CSF dramatically suppressed infection-induced neutrophilia, particularly during early-phase (first 60 min) infection (Fig. 2 A). PB neutrophilia can also be affected by the rate of neutrophil recruitment to the site of inflammation. To assess the effect of G-CSF on neutrophil recruitment to tissues, neutrophils in peritoneal lavage fluid were counted after G-CSF and *E. coli* administration. G-CSF did not affect neutrophil recruitment to the inflamed peritoneal cavity, indicating that the G-CSF–induced reduction in PB neutrophilia was not caused by changes in neutrophil recruitment (Fig. 2 B).

G-CSF inhibits MIP-2–induced neutrophil mobilization from the BM

G-CSF mobilizes neutrophils by reducing CXCR4 expression on neutrophils and decreasing BM CXCL-12 expression
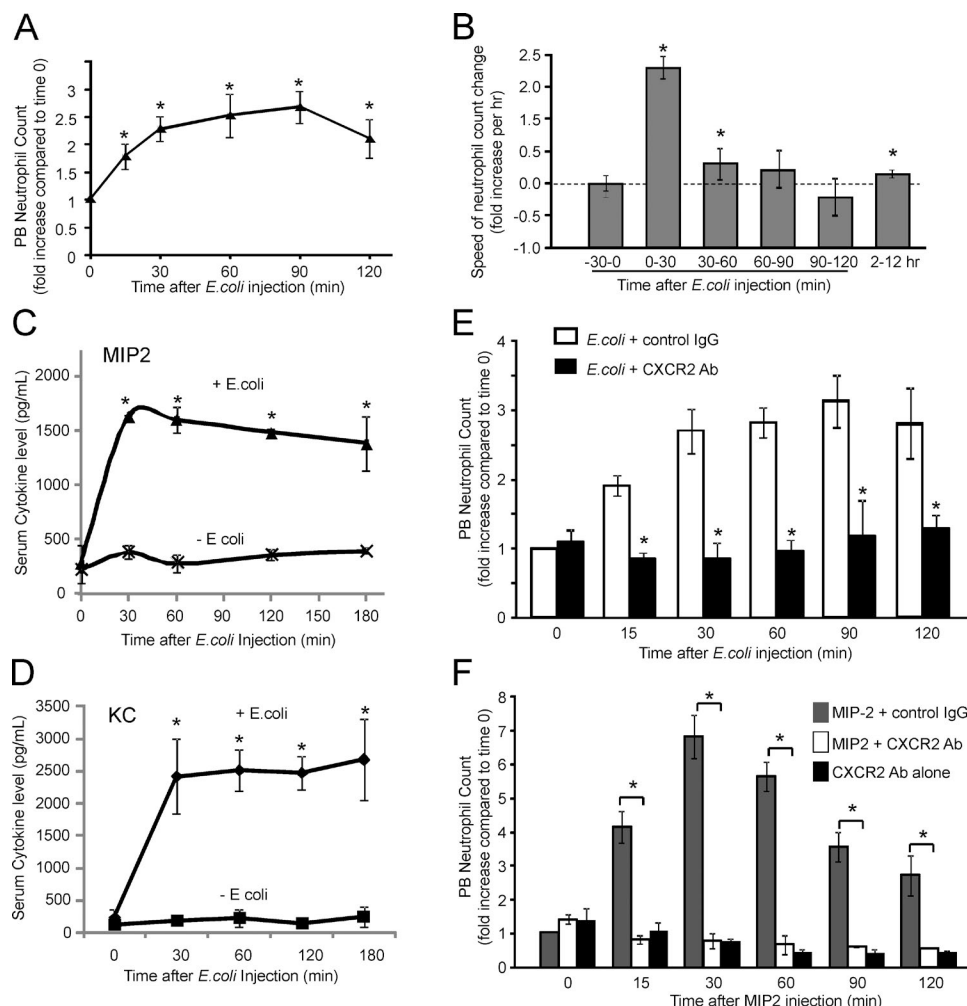
Figure 1. **Rapid neutrophil mobilization in early-stage acute inflammation is mainly mediated by CXCR2 ligands.** (A) Neutrophil counts in PB after *E. coli* administration in the peritonitis model. Changes of PB neutrophil count over time were analyzed by one-way ANOVA–repeated measures. The control group was time 0. (B) The speed of neutrophil count changes at each indicated time period was quantified. The control group was −30 to 0 min. (C) The concentrations of CXCR2 ligand MIP-2 in blood serum. (D) The concentrations of CXCR2 ligand KC in blood serum. The control group was time 0 for each group. Differences over time between groups were analyzed using multivariate ANOVA with measures repeated over time. *E.coli* treatment significantly (P < 0.01) increased serum MIP-2 and KC levels. (A–D) Dunnett's multiple comparison test versus the control group was used. (E) CXCR2 blockade suppresses rapid neutrophil mobilization during early-stage acute inflammation. CXCR2 antibodies or IgG (as control) was i.v. administered to each mouse. (F) CXCR2 ligand MIP-2 induces rapid neutrophil mobilization. MIP-2 (1 µg in 100 µl PBS) and/or CXCR2 antibodies (2 µg in 100 µl PBS) were i.v. administered. (E and F) Student's *t* test versus control (mice treated with IgG) was used. All data are means ± SD of three experiments (*n* = 6 mice). *, P < 0.01. Ab, antibody.

(Semerad et al., 2002, 2005). To further understand the mechanism by which G-CSF regulates blood neutrophilia during acute infection, we monitored the direct effect of G-CSF and MIP-2 alone and in combination on neutrophil mobilization from the BM (Fig. 3 A). As early as 15 min after MIP-2 injection, PB neutrophil numbers were drastically elevated compared with vehicle control (PBS), reaching a maximum at 30 min and returning to basal levels ∼2 h after injection. Conversely, G-CSF significantly reduced circulating neutrophil numbers and induced neutropenia 15 min after injection. This neutropenia was transient, as circulating neutrophil numbers increased after 15 min to reach normal levels by ∼30 min

and continued to elevate thereafter (Fig. 3 A), in agreement with previous observations that circulating neutrophils decrease after a single G-CSF dose and then recover to normal levels (Gordon et al., 2007; DeJesus et al., 2011). Neutrophils appearing in the PB after MIP-2 stimulation originate from the BM; therefore, we counted BM neutrophils 60 min after MIP-2 or G-CSF injection. MIP-2–treated mice had reduced BM neutrophil counts compared with G-CSF–treated mice (Fig. 3 B), consistent with the less significant neutrophilia observed in G-CSF–treated mice during early-stage infection. MIP-2 injection also increased circulating blood eosinophils (Fig. 3 C) but not monocytes or other cell types (Fig. 3 D).
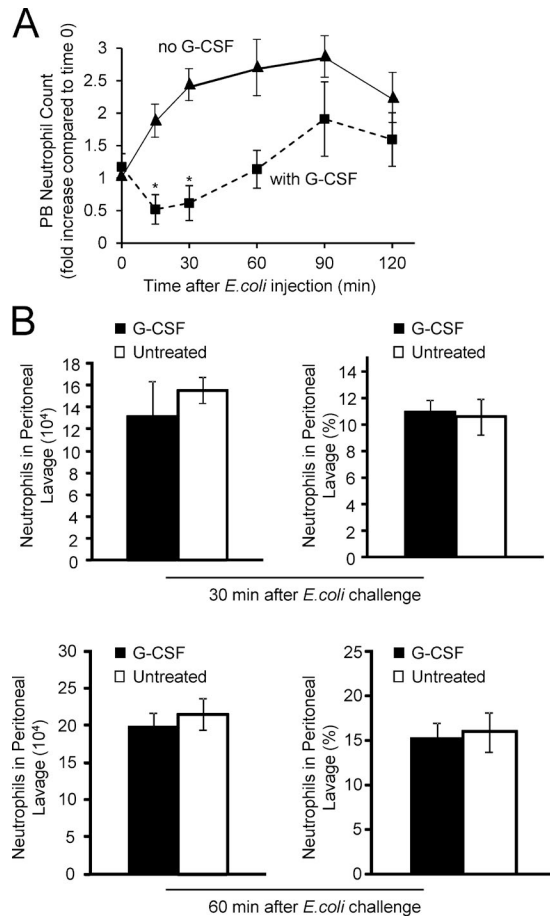
A

B

Figure 2. G–CSF inhibits rapid neutrophil mobilization from the BM during early–stage acute inflammation. (A) G-CSF inhibits *E. coli*–induced rapid neutrophil mobilization. G-CSF (2 µg in 200 µl PBS) and *E. coli* (2 million in 1 ml PBS) were simultaneously injected i.p. into C57BL/6 mice. *, P < 0.01 by Student's *t* test versus control (mice not treated with G-CSF at each time points). (B) G-CSF treatment does not affect neutrophil recruitment to the inflamed peritoneal cavity. Neutrophil counts in the peritoneal lavage were measured at 30 and 60 min after *E. coli* administration. *n* = 10 mice for each group. All data are means ± SD of three experiments.

To address whether G-CSF and MIP-2 synergistically mobilize neutrophils from the BM reservoir, mice were simultaneously injected with MIP-2 and G-CSF. This resulted in significantly lower circulating neutrophil numbers compared with mice injected with MIP-2 alone (Fig. 3 A). At 15 min after administration of this cocktail, circulating neutrophil numbers were even lower than in vehicle-treated controls. Thus, G-CSF appears to play a negative role in infection-induced neutrophilia by inhibiting CXCR2 ligand–mediated neutrophil mobilization from the BM. MIP-2–induced eosinophilia was also inhibited by G-CSF (Fig. 3 C). The goal of this study is to demonstrate that G-CSF can inhibit MIP-2–elicited neutrophil mobilization from the BM. Thus, we used a 1 µg/mouse dose of MIP-2 that could induce the maximal release of neutrophils from the BM with the least variation. This dose

is similar to the optimal dose used by several other laboratories (McColl and Clark-Lewis, 1999; Liu et al., 2007; Wengner et al., 2008). It is higher than the endogenous MIP-2 levels elicited by *E. coli* infection. This may be because of the low bioactivity of recombinant MIP-2 protein.

The inhibitory effect of G-CSF on MIP-2–induced neutrophil mobilization seems to be specific. We explored whether other neutrophil-mobilizing agents had the same effect on MIP-2–induced neutrophil mobilization. AMD3100 is a small molecule antagonist of CXCR4 that is known to induce rapid neutrophilia (Broxmeyer et al., 2005). In contrast to G-CSF, coadministration of MIP-2 and AMD3100 further increased circulating neutrophil numbers compared with MIP-2 or AMD3100 alone (Fig. 3 E).

G–CSF decreases neutrophil mobility in the BM during MIP–2–induced neutrophil mobilization

To directly visualize neutrophil mobilization from the BM, multiphoton intravital microscopy (IVM [MP-IVM]) was used to monitor individual neutrophils in cranial BM. Mice expressing enhanced GFP (eGFP) under the control of the lysozyme M promoter (LysM-eGFP) were used to visualize eGFP-expressing neutrophil kinetics in the BM. This technique enables simultaneous visualization of the blood vessels and neutrophil behavior in the BM under homeostatic conditions and during mobilization in response to an injected mobilizing agent. eGFP was only expressed in myeloid cells in LysM-eGFP mice, the vast majority being mature neutrophils, with eGFP expressed at much lower levels in other myeloid lineages such as macrophages and a subset of dendritic cells (Faust et al., 2000; Chtanova et al., 2008; Peters et al., 2008). In addition, neither MIP-2 nor G-CSF had a significant effect on monocyte mobilization (Fig. 3 D); thus, the majority of migrating GFP^{+} cells detected here were neutrophils. Consistently, immunostaining of the BM slides showed that all GFP^{+} cells were positive for Ly6G, a specific marker for neutrophils (Fig. 4 A).

Treating mice with a single dose of recombinant mouse MIP-2 significantly increased neutrophil mobilization and migration toward blood vessels within 15 min (Fig. 4, B–D and Videos 1 and 2). Neutrophil displacement, velocity, directionality, and upward directionality toward blood vessels increased rapidly after MIP-2 injection (Fig. 4, E–H). On average, ~50% of neutrophils entered blood vessels after MIP-2 injection in MIP-2–treated mice during the 60-min interval, with most entering the circulation 15–25 min after injection (Fig. 4, I–J; and Videos 1 and 2). In this experiment, we tracked each single cell using MP-IVM until it entered the vessels or until the end of the video (Fig. 4, C and D). The imaging depth of MP-IVM was 100 µm. We started the recording at a z depth of ~50 µm and recorded 50–60 µm in the z direction at 5 µm/section. Some cells would migrate in and out of the focal plane during the recording, but these cells could still be visu-
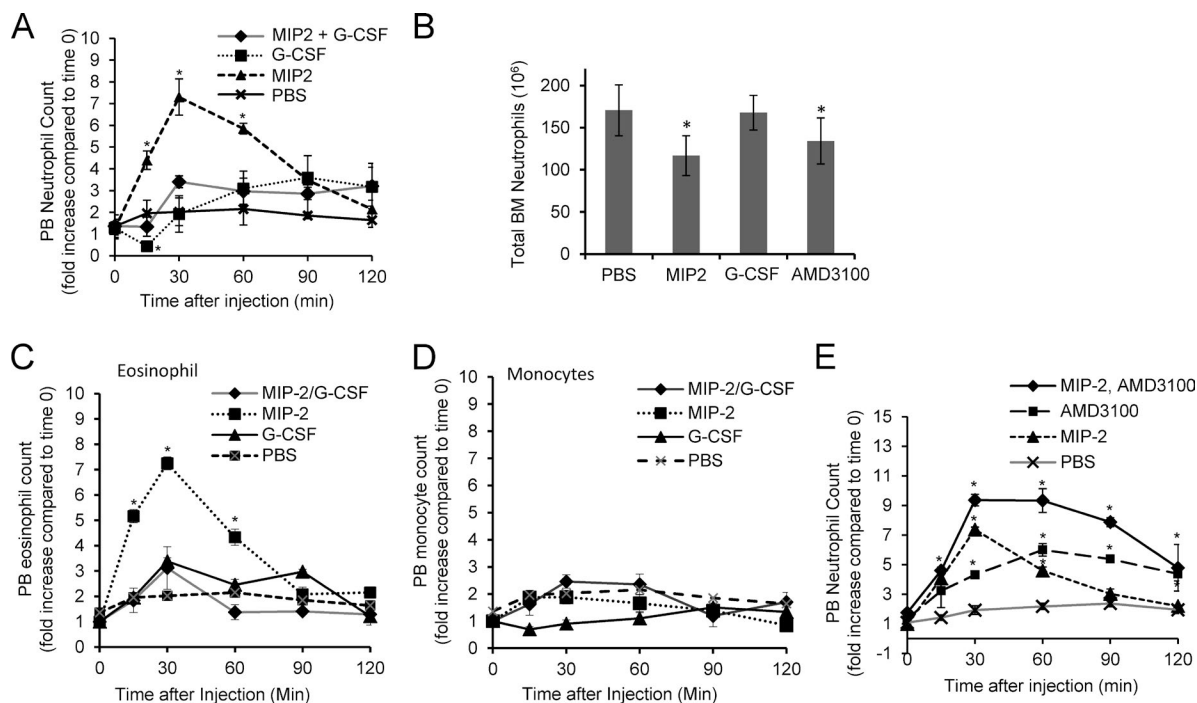
2002

Negative regulation of CXCR2 signaling by G-CSF | Bajrami et al.

Figure 3. **G–CSF specifically inhibits MIP-2–induced neutrophil mobilization from the BM.** (A) MIP-2–induced neutrophil mobilization from the BM in the presence or absence of G-CSF. C57BL/6 mice were i.v. injected with the indicated cytokines. (B) Total numbers of neutrophils remaining in the BM 60 min after each treatment. AMD3100 is a small molecule antagonist of CXCR4. (C) MIP-2 induces eosinophil mobilization. (D) MIP-2 does not have a significant effect on monocyte mobilization from the BM. (E) CXCR4 antagonist AMD3100 further enhances MIP-2–induced neutrophil mobilization. Mice were i.v. injected with 1 µg MIP-2, 2.5 µg G-CSF, or 0.05 mg AMD3100 as indicated. All data shown are means ± SD of three experiments (n = 10 mice for each group). *, P < 0.01 by Student's t test versus control (mice treated with PBS at each time point).

alized under the microscope. We confirmed that the cells that were not seen by the end of the video were indeed those that entered circulation. These cells were not present even when we looked at each single optical sections (image stacks) of the three-dimensional projections, indicating that these cells most likely entered the circulation.

A very different effect was observed in mice treated with G-CSF. Although neutrophil displacement and velocity increased in G-CSF–treated mice (Fig. 4, E and F; and Video 3), there was no specific directionality (Fig. 4, G and H), and the cells did not enter circulation until 55–60 min after G-CSF injection (Fig. 4 I). Even then, only ~20% of eGFP+ neutrophils entered the circulation (Fig. 4 J). Earlier experiments (Fig. 3 A) showed that G-CSF inhibited MIP-2–induced mobilization in mice simultaneously injected with G-CSF and MIP-2, and a similar phenomenon was observed by IVM (Video 4). When mice were simultaneously injected with G-CSF and MIP-2, the neutrophils failed to reach velocities comparable with those in mice treated with MIP-2 alone (Fig. 4, E and F). As in G-CSF–treated mice, neutrophils in mice treated with G-CSF and MIP-2 lost directionality and entered the blood circulation much later than those in mice treated with MIP-2 alone (Fig. 4, G–J). Thus, the MP-IVM approach further demonstrates that G-CSF inhibited MIP-2–induced mobilization of neutrophils from the BM.

G-CSF inhibits MIP-2–elicited neutrophil chemotaxis

In vivo experiments showed that MIP-2 failed to efficiently mobilize neutrophils when the mice were simultaneously treated with G-CSF, suggesting that G-CSF may negatively regulate MIP-2. MIP-2 is a neutrophil chemoattractant that plays a critical role in neutrophil recruitment in response to infection and inflammation. Therefore, we investigated whether G-CSF impaired neutrophil chemotaxis in an MIP-2 gradient using the EZ-TAXIScan apparatus, in which a stable chemoattractant gradient is formed in a 260-µm–wide channel, enabling direct visualization of neutrophil chemotactic migration. Mouse BM neutrophils were exposed to an MIP-2 gradient generated in the presence or absence of G-CSF, and cell movement was recorded by time-lapse microscopy and analyzed. Neutrophils migrated robustly in an MIP-2 gradient (Fig. 5, A–E; and Video 5). However, the presence of G-CSF in the chemotactic gradient severely reduced MIP-2–induced chemotaxis, with neutrophils showing defective directionality and lower migration speed (Fig. 5, A–E; and Video 6). It is noteworthy that G-CSF was not in itself a chemoattractant and did not affect neutrophil mobility when applied alone (Fig. 5, A–E; and Video 7). In addition, the effect of G-CSF was unique to CXCR2-mediated neutrophil chemotaxis. G-CSF did not affect chemotaxis elicited by other chemoattractants such as LTB4, C5a, or fMLP
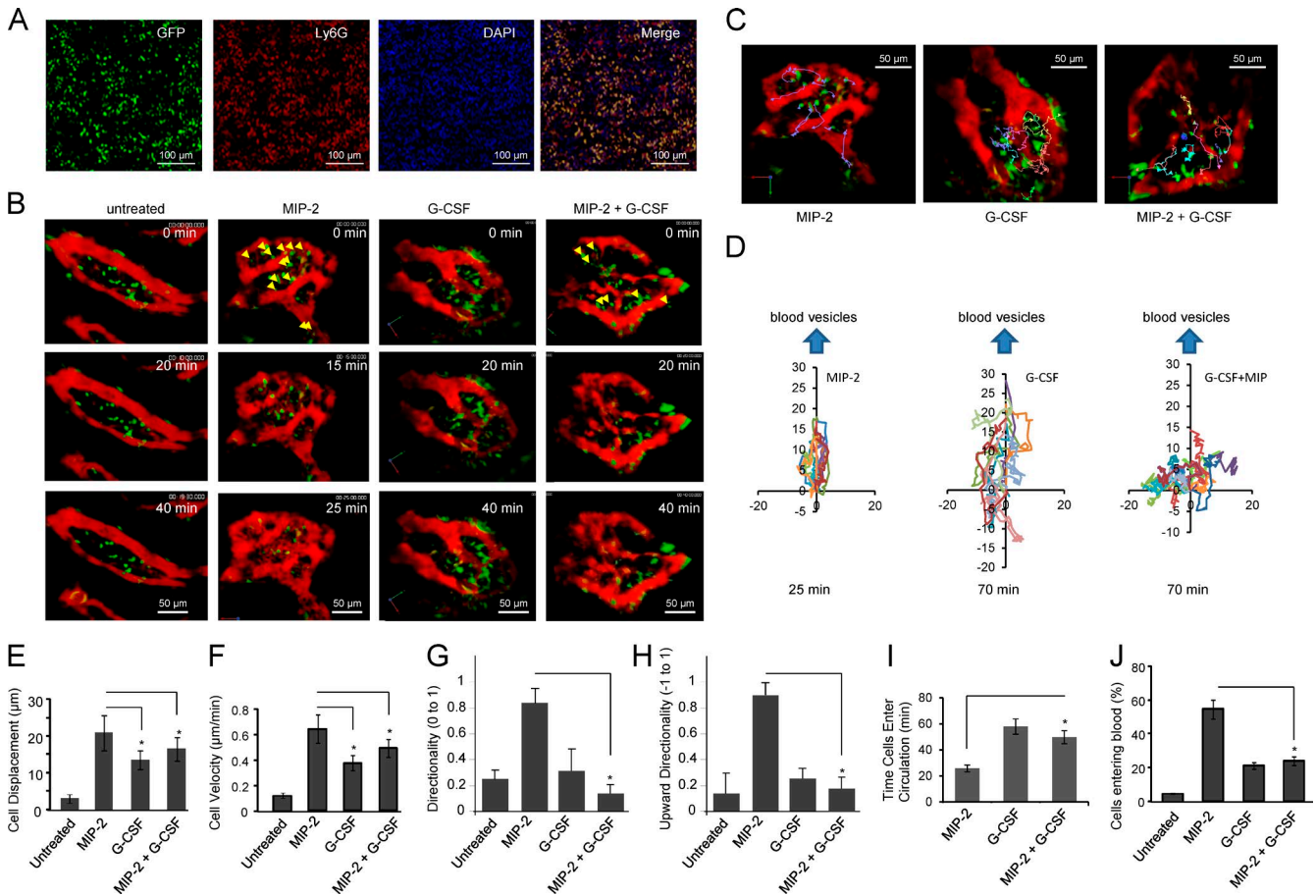
Figure 4.   **MIP–2–induced neutrophil mobilization from the BM is hindered in the presence of G–CSF.** (A) GFP^{+} cells in LysM-eGFP mice are positive for Ly6G, a specific marker for neutrophils. Data shown are representative of four experiments with similar results. (B–J) Transgenic mice expressing eGFP under the control of the LysM promoter were i.v. injected with 1 µg MIP-2 or/and 2 µg G-CSF. The mobilization of GFP^{+} cells was monitored in vivo by MP-IVM (also see Videos 1, 2, 3, and 4). (B) Microscopy images at the indicated time points. Representative images from four independent experiments are shown. Arrows indicate neutrophils (time 0) that left upon the treatment. (C) Microscopy images illustrating the migratory patterns of neutrophils (GFP^{+} cells) in the parenchyma and sinusoids of calvarium BM in the first 25 (for MIP-2 alone) or 70 (for G-CSF and G-CSF + MIP-2) min after administration of the indicated cytokines. The tracks of several motile cells are shown. Tracks are sometimes partial because of the depth of the projected image. Bars: (A) 100 µm; (B and C) 50 µm. (D) Tracks of GFP[+] neutrophils in the BM parenchyma, illustrating the different migrating patterns toward the blood vessels (y axis). GFP[+] neutrophils were tracked after stimulant administration until they entered the vessels or until the end of the video (25 min for MIP-2 and 70 min for G-CSF and G-CSF + MIP-2). Tracks were obtained from IVM images and are illustrated as starting from a common starting point. (E) Displacement of parenchymal and sinusoidal GFP[+] neutrophils in the first 25 (for MIP-2 alone) or 70 (for G-CSF and G-CSF + MIP-2) min after administration of the indicated cytokines. Total cell displacement was measured from the position at which each cell started at the beginning of the observation period to its location at the end of the recording. (F) Velocity of parenchymal and sinusoidal GFP[+] neutrophils. (G) Directionality of neutrophils. (H) Upward directionality. (I) The mean time taken by GFP[+] neutrophils to migrate from the parenchyma into the blood vessels after the indicated treatments. (J) Percentage of migrating GFP[+] neutrophils that entered the circulation in the first 60 (for MIP-2 alone) or 70 (for G-CSF and G-CSF + MIP-2) min after administration of the indicated cytokines. Data shown are means ± SD of three experiments (n = 4–6 mice). *, P < 0.01 versus mice treated with MIP-2 alone.

(Fig. 5 F and Videos 8 and 9). Similar results were observed in both mouse and human neutrophils (Fig. 5 G). Collectively, these results demonstrate that G-CSF can specifically negatively modulate MIP-2–mediated neutrophil chemotaxis.

G-CSF negatively regulates MIP-2–induced signaling
G-CSF treatment suppressed PB neutrophilia induced by *E. coli* but did not alter KC and MIP-2 levels, eliminating the possibility that G-CSF suppressed infection-associated neu-

trophilia by down-regulating CXCR2 ligand levels (Fig. 6 A). Consistent with this, in an in vitro assay, G-CSF directly inhibited MIP-2–elicited neutrophil chemotaxis. These results suggest that G-CSF regulates neutrophil function by modulating MIP-2–induced intracellular signaling.

Neutrophils use various signaling cascades during chemotaxis including PI3K/Akt and MAPK signaling. Neutrophil stimulation with MIP-2 induced robust phosphorylation of Erk1/2 and Akt. Interestingly, G-CSF dramatically reduced
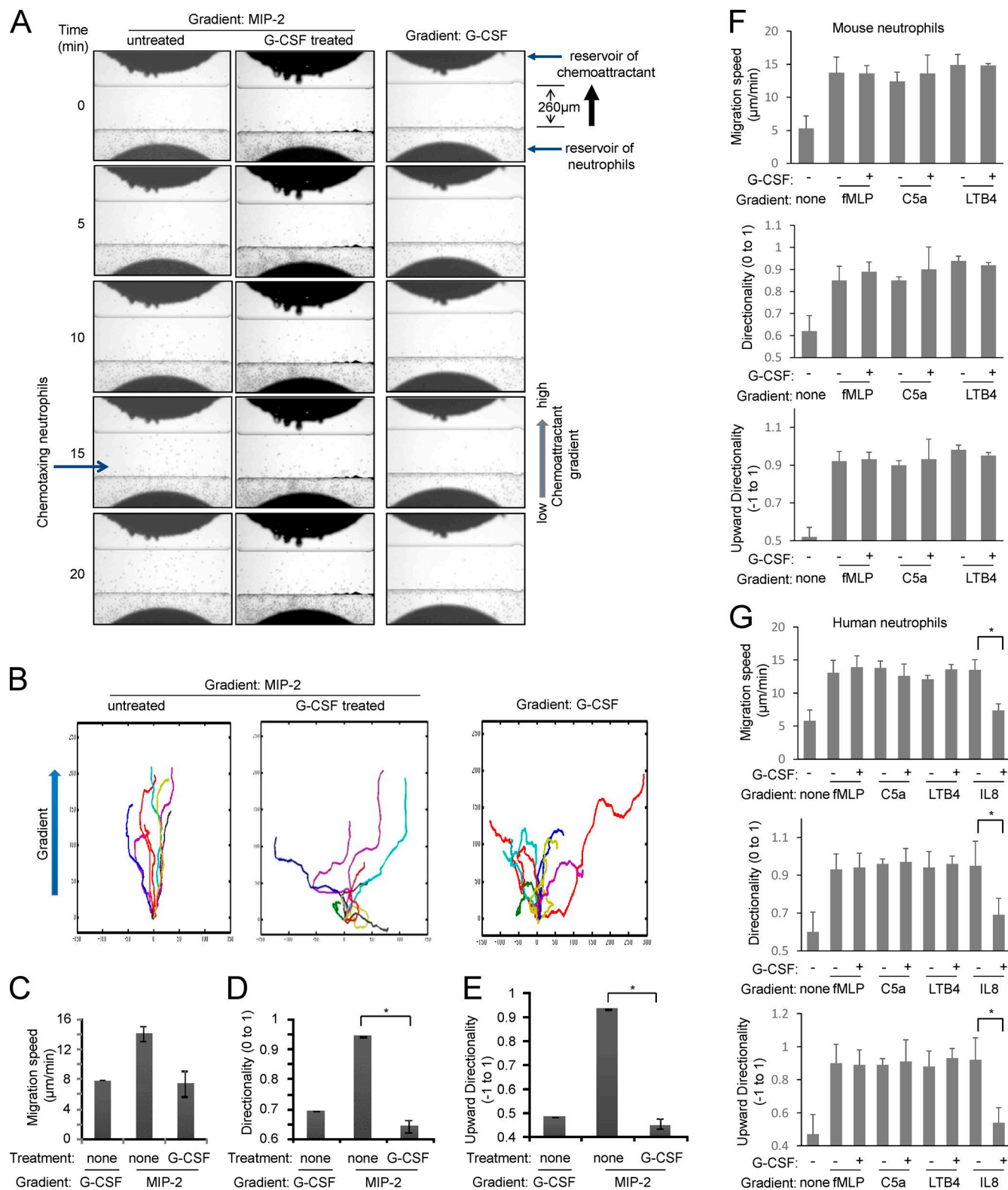
Figure 5. **G-CSF inhibits MIP-2–induced neutrophil chemotaxis.** (A) Chemotaxis of untreated or G-CSF–treated mouse neutrophils (also see Videos 5, 6, and 7). (B) Tracks of migrating neutrophils (cells that moved at least 65 μm from the bottom of the channel; *n* = 10) were traced from the captured images, realigned such that all cells started from the same starting point (0,0), and plotted. Chemoattractant concentration increases in the positive y direc-

MIP-2–elicited Erk1/2 phosphorylation but not Akt phosphorylation (Fig. 6, B and C). G-CSF signaling is mediated by phosphorylation and activation of STAT3 by the nonreceptor tyrosine kinase Janus kinase 2 (JAK2). G-CSF treatment rapidly increased STAT3 phosphorylation in neutrophils. To explore whether G-CSF–induced STAT3 activation is essential for suppression of MIP-2–elicited signaling, we investigated the effect of a JAK2 inhibitor, INCB018424, which completely inhibited STAT3 phosphorylation (Fig. 6, D and E). Blocking STAT3 phosphorylation with INCB018424 inhibited the reduction in Erk1/2 phosphorylation in neutrophils stimulated with MIP-2 and G-CSF (Fig. 6 F) and also reversed G-CSF–induced neutrophil chemotaxis defects in the MIP-2 gradient (Fig. 6, G–K; and Videos 6 and 10). Collectively, these results indicate that G-CSF–induced STAT3 signaling negatively regulates MIP-2–elicited Erk1/2 signaling, which in turn regulates neutrophil chemotaxis.

Endogenously produced G–CSF negatively regulates rapid neutrophil mobilization at the early stage of acute infection

G-CSF is a hematopoietic cytokine generated by monocytes, macrophages, fibroblasts, and endothelial cells that is elevated by sepsis/severe bacterial infection in multiple clinical studies (Anderlini et al., 1996; Liu et al., 1996; Basu et al., 2002; Cottler-Fox et al., 2003; Gregory et al., 2007; Greenbaum and Link, 2011). However, based on our ELISA results and previously published work (Metcalf et al., 1996), G-CSF increases later than KC or MIP-2 after *E. coli*–induced peritonitis. The levels of the CXCR2 ligands KC and MIP-2, but not G-CSF, rapidly increased in serum, peaking at 30 min after i.p. injection of *E. coli* (Fig. 1, B and C). In contrast, serum G-CSF levels began to increase 60 min after *E. coli* injection, peaking at 2 h (Fig. 7 A). To specifically investigate the function of endogenously produced G-CSF in *E. coli*–induced peritonitis, mice were treated with a monoclonal anti–mouse G-CSF antibody for 1 h before *E. coli* infection (Fig. 7 B). Circulating neutrophil counts were significantly elevated in mice treated with a G-CSF–blocking antibody. G-CSF antibody failed to augment neutrophil counts in mice treated with PBS alone, indicating that its effect was dependent on *E. coli*–elicited inflammation (Fig. 7 C). Neutrophil counts were also measured in the BM: mice treated with G-CSF–blocking antibodies contained significantly less BM neutrophils both 2 and 6 h after *E. coli* injection, confirming that the elevated PB counts were a result of augmented neutrophil mobilization from the BM (Fig. 7 D). Finally, more neutrophils were also observed in the peritoneum of G-CSF antibody–treated mice both 2 and 6 h after *E. coli* administration (Fig. 7 E), which may be the result of the peripheral neutrophilia observed in these mice. These results suggest that endogenously produced

G-CSF during acute infection not only negatively regulates rapid neutrophil mobilization during early-stage infection, but also controls neutrophil recruitment to the site of inflammation by modulating PB neutrophils.

Of note, treatment with G-CSF–blocking antibodies did not alter *E. coli*–induced elevation of MIP-2 and KC levels in the serum, confirming that G-CSF regulates neutrophil mobilization by modulating CXCR2-elicited signaling rather than altering CXCR2 ligand levels (Fig. 7 F).

Endogenous G-CSF prevents systemic neutrophil extravasation

Activation of PB neutrophils by chemokines and/or cytokines is a prerequisite for neutrophil recruitment to infected tissues. However, uncontrolled neutrophil activation and/or elevated PB neutrophil counts may lead to systemic neutrophil extravasation and unwanted inflammation. Because endogenously produced G-CSF negatively regulates MIP-2–elicited signaling and rapid neutrophil mobilization during early-stage acute infection, this may be an important mechanism to prevent systemic neutrophil extravasation during infection. To test this hypothesis, we suppressed G-CSF function using G-CSF–blocking antibodies and examined neutrophil accumulation in the lungs after injecting i.p. *E. coli* (Fig. 8 A).

Neutrophil accumulation in the lungs was assessed 6 h after bacterial injection using bronchoalveolar lavage (BAL; Fig. 8, B–D) and histological morphometric analysis of lung sections (Fig. 8, E–G). i.p. *E. coli* injection does not usually recruit neutrophils to the lungs, and as expected, very few neutrophils were detected in the lungs of unchallenged mice and mice challenged with i.p. injection of *E. coli* or i.v. injection of IgG. However, when G-CSF–blocking antibodies were administered with *E. coli*, BAL neutrophils reached nearly 20% (Fig. 8 C) and levels of 3.5×10^5 (Fig. 8 D) 6 h after bacterial injection. A similar accumulation was observed in the lung tissue (Fig. 8 F) and in emigrated neutrophils in alveolar air spaces (Fig. 8 G) in histological sections quantified by morphometry.

Inflammation is associated with the release of cytokines and chemokines at the site of infection, which subsequently induce the accumulation and activation of neutrophils, monocytes/macrophages, and lymphocytes. Lung cytokine and chemokine levels increased in mice challenged by i.p. injection of *E. coli* and i.v. injection of G-CSF–blocking antibodies (Fig. 8 H). The proinflammatory cytokines/chemokines IL-1α, IL-1β, IL-6, MIG/CXCL9 (monokine induced by γ interferon), and MCP-1 (monocyte chemoattractant protein 1) were increased in the BAL fluid (BALF) of anti–G-CSF antibody–treated mice. IL-1β was most elevated, showing approximately sevenfold-higher expression

---

tion. (C–E) Tracks of migrating neutrophils were analyzed to determine directionality, upward directionality, and migration speed. (F) G-CSF does not affect chemotaxis elicited by LTB4, C5a, and fMLP in mouse neutrophils (also see Videos 8 and 9). (G) G-CSF specifically suppresses MIP-2–mediated chemotaxis of human neutrophils. Data are represented as means ± SD of three experiments (*n* = 20 cells). *, P < 0.01 versus neutrophils not treated with G-CSF.

2006

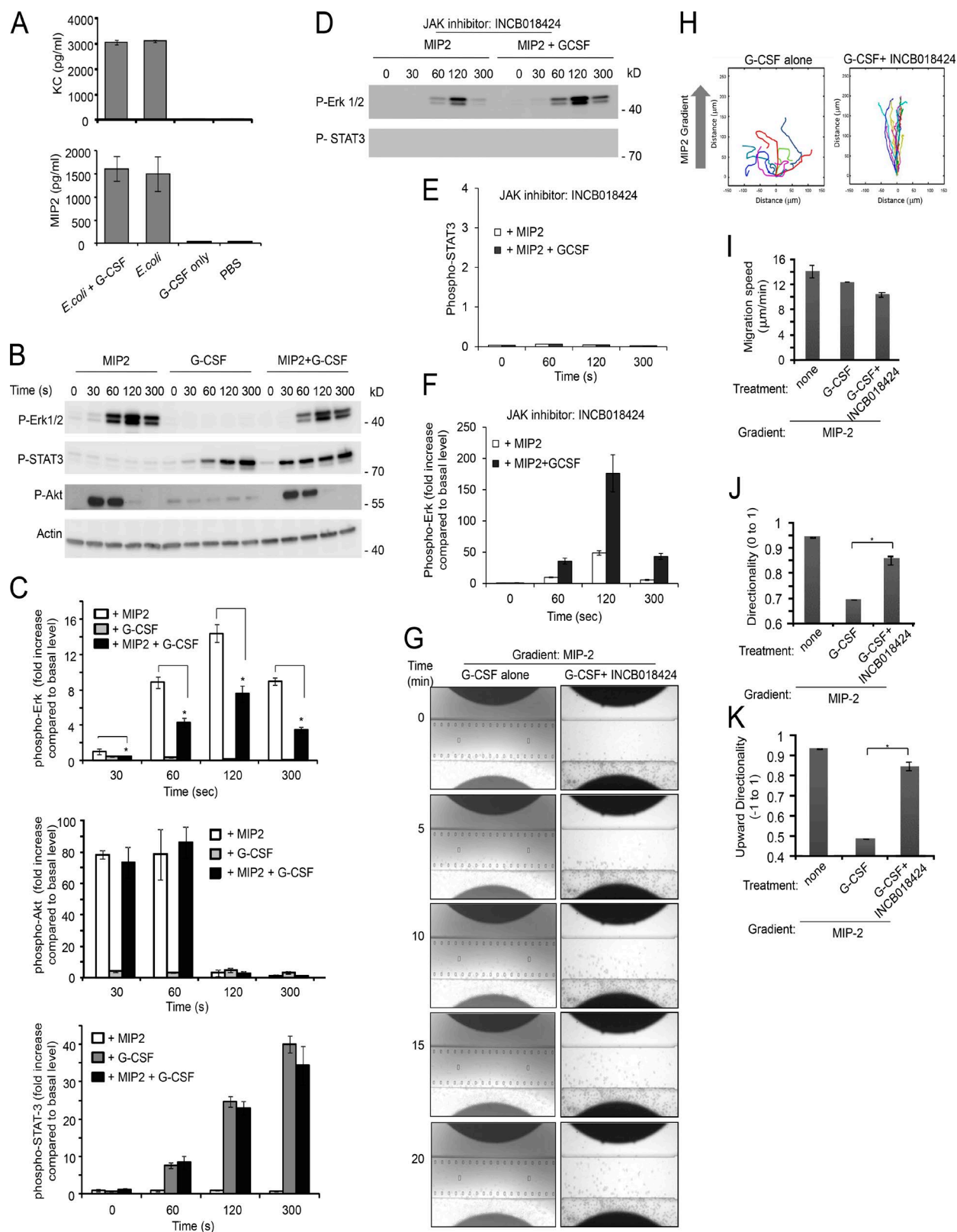Negative regulation of CXCR2 signaling by G-CSF | Bajrami et al.

Figure 6. **The inhibitory effect of G–CSF is mediated by activation of STAT3 signaling and the subsequent suppression of MIP–2–elicited cell signaling.** (A) G–CSF treatment does not alter the KC and MIP-2 serum levels in mice i.p. injected with *E. coli*. Mice were i.p. injected with 2 ×10^{6} CFU *E. coli* and/or i.v. injected with 2 µg G-CSF. Data shown are representative of three experiments (*n* = 5 mice). (B) Mouse BM neutrophils were stimulated with

in G-CSF antibody–treated mice. The elevation of cytokine levels induced by G-CSF blockage was likely a result of the enhanced neutrophil recruitment because depletion of neutrophils with anti-Gr1 antibody abolished this G-CSF antibody–elicited effect (Fig. 8, I and J). However, the cytokine levels in the lungs remained high even in neutrophil-depleted mice, indicating that neutrophils were not the direct source of cytokine production. Collectively, these results indicate that G-CSF blockade in mice challenged with i.p. *E. coli* leads to neutrophil accumulation and inflammation in the lungs.

Blocking G-CSF aggravates LPS–induced lung injury
Exaggerated neutrophil accumulation can lead to tissue damage. Endogenously produced G-CSF negatively regulates CXCR2-mediated rapid neutrophil mobilization and activation during infection. Thus, blocking G-CSF may enhance neutrophil recruitment at the site of infection by increasing PB neutrophils and augmenting their activation. We tested this hypothesis in an LPS-induced acute lung inflammation model (Fig. 9 A). Neutrophil accumulation and edema formation in inflamed lungs was assessed 6 h after intratracheal LPS instillation by BAL and morphometric analysis of lung sections. As expected, very few neutrophils were observed in untreated mice. Instillation of LPS induced significant neutrophil accumulation in the lungs. Treatment with G-CSF–blocking antibodies further elevated neutrophil accumulation (Fig. 9, B–D). Approximately twice as many neutrophils were present in the alveolar air spaces of mice treated with G-CSF antibodies (Fig. 9 C). The number of neutrophils in the BALF of G-CSF antibody–treated mice was also higher after LPS instillation compared with IgG antibody–treated control mice (Fig. 9 D).

Increased numbers of neutrophils in the lungs can lead to tissue damage and edema (Doerschuk, 2000). Edema was formed in mouse lungs after LPS treatment. Consistent with elevated neutrophil recruitment, greater edema formation was noted in the lungs of mice treated with G-CSF antibodies (Fig. 9 E). Lung damage is often accompanied by vascular leakage, and increased BAL protein levels are used as an indicator of vascular leakage and a surrogate of inflammatory lung injury. We consistently detected augmented pulmonary protein accumulation in the lungs of G-CSF antibody–treated mice (Fig. 9 F), again confirming that G-CSF–blocking antibody treatment exaggerates LPS-induced lung inflammation.

Increasing the dose of instilled LPS from 0.5 to 2 mg/kg further induced neutrophil recruitment, edema formation, and vascular leakage in both G-CSF antibody–treated and isotype control-treated mice (Fig. 9, C–E). The effect of G-CSF antibodies was observed under all experimental conditions used in the current study.

Collectively, these results indicate that endogenously produced G-CSF plays a critical role in negatively regulating neutrophil recruitment in acute lung inflammation, thus preventing exaggerated neutrophil accumulation and inflammation-induced lung damage. Disrupting G-CSF signaling enhances neutrophil accumulation in the lungs, edema formation, and severe lung inflammation in LPS-treated mice.

DISCUSSION
Neutrophil homeostasis is maintained, in part, by their regulated release from the BM. The chemokine CXCL12 (stromal cell–derived factor 1), by interacting with its major receptor CXCR4, plays a critical role in controlling neutrophil mobilization and homeostasis under both basal and stress granulopoiesis conditions (Martin et al., 2003; Suratt et al., 2004; Eash et al., 2009, 2010; Petty et al., 2009). In addition to CXCR4, CXCL2/CXCR2 signaling is considered to be a second chemokine axis required for neutrophil mobilization (Eash et al., 2010). CXCR2 ligands stimulate neutrophil mobilization in a VAL4-dependent manner (Burdon et al., 2005). Based on a proposed tug-of-war model, CXCL2/CXCR2 signals and CXCL12/CXCR4 signals act antagonistically to regulate neutrophil retention in and release from the BM (Eash et al., 2010). In the current study, we show that CXCR2 ligands MIP-2 and KC were quickly expressed during acute inflammation and were responsible for initial rapid neutrophil mobilization. The concentrations of CXCR2 ligands continued to increase during inflammation; however, the speed of neutrophil mobilization slowed after the initial acute fast phase. We demonstrate that this slowing of neutrophil release is caused by suppression of CXCR2-mediated signaling by G-CSF.

G-CSF is a prototypical neutrophil-mobilizing cytokine. G-CSF–induced down-regulation of CXCR4 expression is one mechanism for mobilization of myeloid cells (Nagase et al., 2002; Kim et al., 2006). Humans and mice treated with AMD3100, a selective CXCR4 antagonist, or CXCR4-blocking antibodies undergo rapid PB neutrophilia (Broxmeyer, 2008; Eash et al., 2009). The CXCR4 antago-
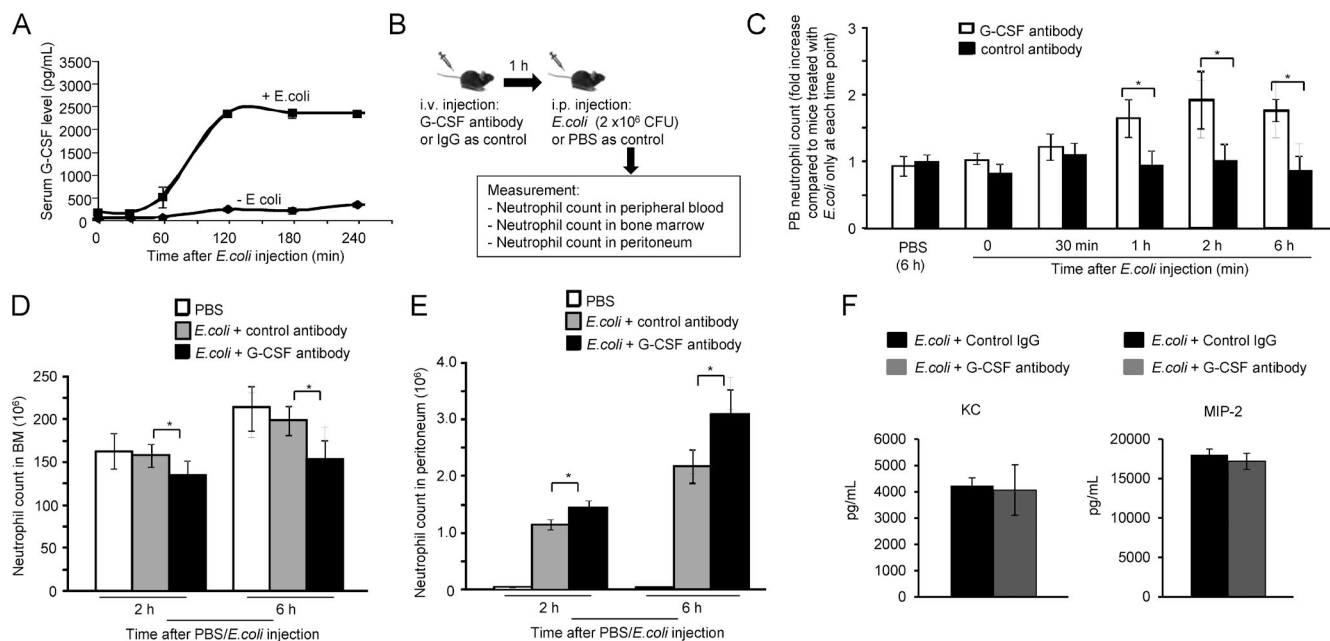
Figure 7. **Blocking G–CSF increases rapid neutrophil mobilization during early–stage acute inflammation.** (A) The G-CSF concentration in blood serum after administration of *E. coli*. 10^6 CFU *E. coli* or PBS (as control) was i.p. injected. (B) Mice were treated with 100 µg G-CSF antibody for 1 h before administration of *E. coli*. IgG was administered to the control group. (C) PB neutrophil counts were measured using a HemaVet 850 hematology system. Fold increases compared with mice treated with *E. coli* only (or PBS only as a control) at each time point are shown. (D) Total number of neutrophils in the BM. (E) The number of neutrophils in peritoneal lavage was measured by flow cytometry analysis 2 and 6 h after *E. coli* administration. (F) Blocking G-CSF activity does not alter KC and MIP-2 levels in mice i.p. injected with *E. coli*. n = 4–6 mice. Data shown are means ± SD of three experiments. *, P < 0.01 versus mice treated with IgG.

nist plerixafor can also correct leukopenia in patients with warts, hypogammaglobulinemia, infections, and WHIM (warts, hypogammaglobulinemia, immunodeficiency, and myelokathexis) syndrome (Dale et al., 2011; McDermott et al., 2011, 2014). It is noteworthy that a recent study indicated that plerixafor-mediated CXCR4 inhibition does not mobilize neutrophils from the BM. Instead, it elicits neutrophilia by promoting neutrophil release from the marginated pool present in the lung and preventing neutrophil circulation back to the BM (Devi et al., 2013). This demargination is likely to be caused by increased neutrophil blood velocities and decreased endothelium–neutrophil interactions (Doerschuk et al., 1988). A recent study also suggested that autophagy plays a role in G-CSF–elicited stem cell mobilization (Leveque-El Mouttie et al., 2015).

Here, we found that G-CSF was expressed after MIP-2 and KCs were expressed during acute infection. MIP-2–induced neutrophil mobilization from the BM was hindered by G-CSF, which negatively regulated MIP-2–induced signaling and inhibited MIP-2–elicited neutrophil chemotaxis. Importantly, the effect of G-CSF was unique to CXCR2-mediated chemotaxis. G-CSF did not affect chemotaxis elicited by other chemoattractants such as LTB4, C5a, or fMLP. Thus, G-CSF mainly regulates neutrophil trafficking at the early stage of infection. It would not suppress neutrophil chemotactic migration toward pathogens, a process mainly mediated by fMLP and

C5a. It is well documented that neutrophil chemotaxis can be driven by diverse chemotactic signaling pathways depending on the chemoattractant gradient being exposed to the cells (Foxman et al., 1997; Heit et al., 2002, 2008). The molecular basis underlying the specificity of G-CSF toward CXCR2 ligands is still largely unknown and needs to be further investigated.

Strikingly, despite its well known neutrophil–mobilizing function, endogenously produced G-CSF negatively regulated rapid neutrophil mobilization during early-stage acute infection. Blocking G-CSF in vivo unexpectedly elevated PB neutrophil counts in mice injected i.p. with *E.coli* and resulted in sequestration of large numbers of neutrophils in the lungs and sterile pulmonary inflammation. Finally, we found that endogenously produced G-CSF also played a critical role by negatively regulating neutrophil recruitment in an LPS–induced acute lung inflammation model, thus preventing exaggerated neutrophil accumulation and inflammation-induced lung damage. Blocking G-CSF led to enhanced neutrophil accumulation in the lungs, edema formation, and more severe lung inflammation in LPS-treated mice. This represents a previously undefined mechanism by which G-CSF controls neutrophil mobilization and homeostasis during infection and inflammation. Because both G-CSF and CXCR2 ligands are capable of mobilizing hematopoietic stem/progenitor cells, the mechanism identified here may also play a role in regulating hematopoietic grafts and hematopoiesis.
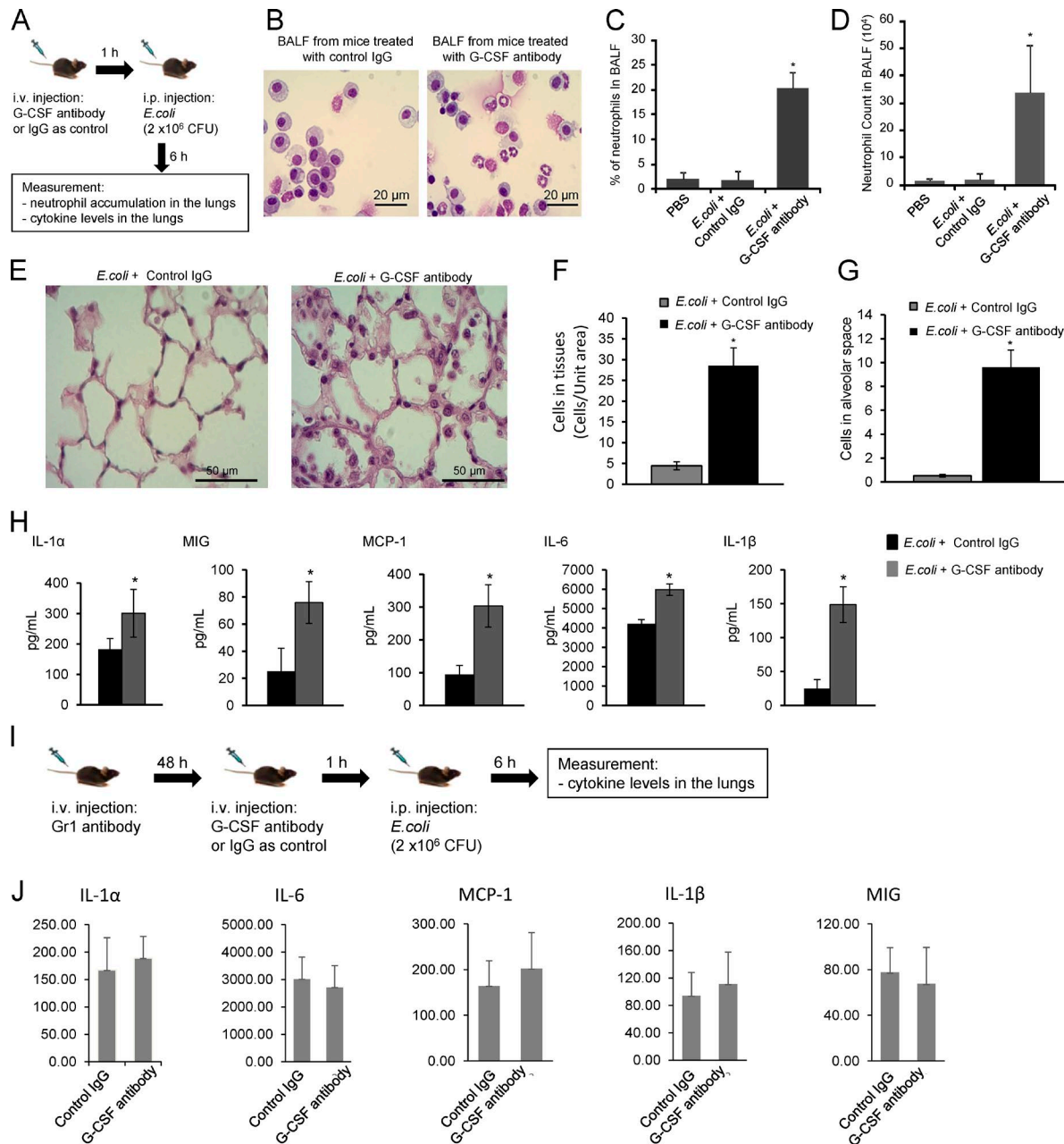
Figure 8. **Blocking G-CSF activity induces neutrophil sequestration in the lungs, leading to sterile pulmonary inflammation in mice i.p. injected with *E. coli*.** (A) Schematic representation of the experimental procedures. (B) Cells in BALF were stained with a modified Wright–Giemsa stain (40× immersion oil). (C) The percentage of neutrophils in BALF. (D) Neutrophil counts in BALF. (E) Staining of lung sections shows emigrated neutrophils in the lungs (20× dry lens). (F) The number of cells in the lung capillaries was quantified as the number of cells in total capillaries (but not alveolar air spaces)/10 alveolar air space area using ImageJ. (G) Emigrated neutrophils in alveolar spaces were quantified as volume fraction of the alveolar air space using standard point-counting morphometric techniques. (H) Cytokine/chemokine levels in BALF were measured using specific ELISA kits. (I and J) G-CSF blockage–induced elevation of cytokine levels in the lungs is mediated by neutrophils. (I) Schematic representation of the experimental procedures. Neutrophils were depleted by a Gr-1 antibody in both PB (∼85% depletion) and the BM (∼65% depletion; Kwak et al., 2015). (J) Cytokine/chemokine levels in BALF. Data shown are means ± SD of three experiments (n = 5 mice). *, P < 0.01 versus control (mice treated with IgG).

Interactions between G-CSF and CXCR2 ligand have been previously investigated. It is proposed that G-CSF–induced neutrophil mobilization is mediated by CXCR2

ligands (Eash et al., 2010; Köhler et al., 2011). CXCR2 ligand expression in megakaryocytes and endothelial cells is up-regulated after G-CSF treatment. In CXCR2-deficient
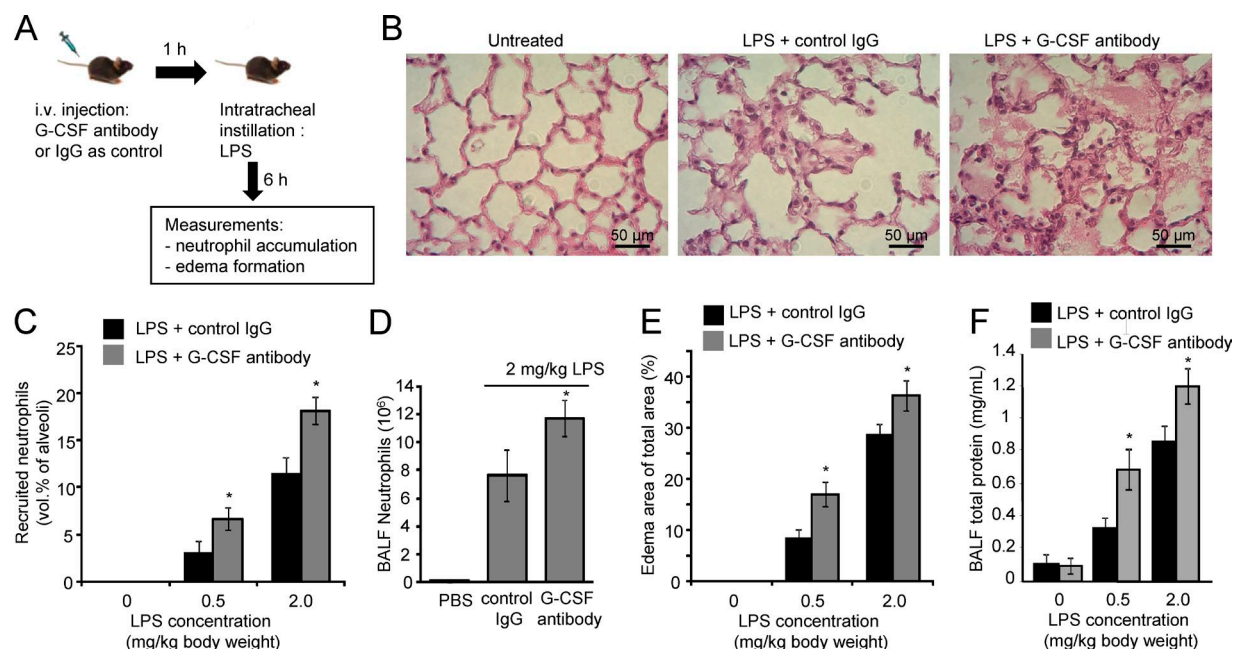
2010

Negative regulation of CXCR2 signaling by G-CSF | Bajrami et al.

Figure 9. **Blocking G-CSF activity aggravates LPS–induced acute lung inflammation.** (A) Schematic representation of the experimental procedures. (B) Staining of lung sections shows emigrated neutrophils and polymerized fibrin in the pulmonary parenchyma. (C) The number of neutrophils emigrating to alveolar air spaces was quantified as volume fraction of the alveolar air space using standard point-counting morphometric techniques. (D) Neutrophil counts in BALF were calculated using the Wright–Giemsa staining method. (E) Pulmonary edema formation. (F) BALF total protein. The standard curve was constructed using BSA. Data shown are means ± SD of four experiments (n = 6 mice). *, P < 0.01 versus control (mice treated with IgG).

mice, G-CSF fails to induce neutrophil mobilization (Eash et al., 2010; Köhler et al., 2011). In contrast, expression of G-CSF can also be regulated by CXCR2. CXCR2 activation on neutrophils by the CXCR2 ligand CXCL5 derived from gut-resident cells negatively regulates IL-17A and G-CSF expression. In the absence of this CXCR2-dependent negative feedback, commensal bacteria can promote IL-17A and G-CSF expression (Mei et al., 2012). Previous studies indicate that G-CSF and CXCR2 ligands synergistically regulate hematopoietic cell mobilization. A single dose of the CXCR2 ligand MIP-2 synergistically enhances hematopoietic stem and progenitor cell mobilization when used in combination with G-CSF, and this effect is dependent on neutrophil-derived MMP-9 (Pelus et al., 2004). However, a later study showed that hematopoietic progenitor cell mobilization by G-CSF was normal in MMP9-deficient mice, suggesting protease-independent pathways may also contribute to hematopoietic progenitor cell mobilization (Heissig et al., 2002; Levesque et al., 2004). Using an in situ perfusion system of mouse femoral BM, Wengner et al. (2008) reported that the CXCR2-selective chemokine KC and G-CSF mobilized significantly more neutrophils when applied together, indicating that these factors act cooperatively to regulate neutrophil mobilization. However, the result was not confirmed in animal models. Paradoxically, here, we observed suppression of MIP-2–induced neutrophil mobilization by G-CSF at early time points (Fig. 3) and clear enhancement

of infection–induced neutrophil mobilization in mice treated with G-CSF–blocking antibody (Fig. 7). We reason that the synergistic effect of G-CSF and CXCR2 ligands only occurs after the acute early phase.

G-CSF is a well known hematopoietic cytokine and a major regulator of neutrophil homeostasis (Anderlini et al., 1996; Liu et al., 1996; Basu et al., 2002; Cottler-Fox et al., 2003; Gregory et al., 2007; Greenbaum and Link, 2011). G-CSF is used clinically to restore neutrophil numbers in neutropenia–related pneumonia patients by stimulating the BM to produce more neutrophils. G-CSF also plays a critical role in homeostatic regulation of neutrophil production by efferocytosis (clearance of apoptotic neutrophils; Bratton and Henson, 2011; Poon et al., 2014). Neutrophil production needs to match neutrophil elimination to maintain approximately constant circulating numbers. Efferocytosis of apoptotic neutrophils in tissues by macrophages and dendritic cells leads to reduced phagocyte secretion of IL-23, a cytokine controlling IL-17 production by γ-δ T cells and unconventional α-β T cells. IL-17, in turn, regulates granulopoiesis through G-CSF (Stark et al., 2005; Smith et al., 2007). The current dogma proposes that G-CSF is an important proinflammatory cytokine (Eyles et al., 2008; Cornish et al., 2009; Vlahos et al., 2010). Our result that G-CSF negatively regulates neutrophil mobilization is somewhat surprising. A similar effect was also observed in an *E. coli* pneumonia model in which G-CSF treatment paradoxically decreased circu-

lating neutrophil counts, resulting in reduced host defense, impaired bacterial killing, and thus aggravated pulmonary injury (Karzai et al., 1999). We demonstrated that G-CSF does not synergize with CXCR2 chemokines to induce neutrophil mobilization during early-phase infection. Instead, it inhibits CXCR2-mediated rapid neutrophil mobilization. In multiple clinical studies, G-CSF is elevated upon sepsis/severe bacterial infection. However, it is produced relatively late compared with KC and MIP-2 in mice. This ensures that the initial CXCR2-mediated neutrophil mobilization can occur at maximal levels without G-CSF–induced inhibition. Rapid release of neutrophils into the circulation then leads to maximal neutrophil recruitment to the site of infection and, in doing so, maximizes the bactericidal capability of the host. At later stages of infection, G-CSF is produced to suppress CXCR2-mediated rapid neutrophil mobilization and to initiate more controlled regulation characterized by accelerated granulopoiesis and G-CSF–mediated slow neutrophil mobilization from the BM.

Although G-CSF has been routinely used to treat neutropenia, transient neutropenia often occurs shortly after G-CSF administration. A recent study suggests that this transient neutropenia is mainly caused by neutrophil accumulation in pulmonary vasculature (DeJesus et al., 2011) and might be mediated by leukocyte integrin activation after G-CSF administration (Donahue et al., 2011). Our results indicate that G-CSF–induced inhibition of CXCR2 signaling may be an alternative mechanism leading to G-CSF–elicited transient neutropenia.

Absolute neutrophil counts in the PB reflect the body's neutrophil supply under normal steady-state conditions. However, when neutrophils are produced under stress conditions such as drug treatment, infection, chemotherapy, or hematopoietic transplantation, neutrophil tissue repopulation and functional capacity becomes a more reliable proxy for neutrophil supply and restoration of innate immune protection (Cheretakis et al., 2006; Devi et al., 2013). CXCR2-mediated cell signaling is important for not only neutrophil mobilization from the BM, but also for various neutrophil functions such as polarization, reactive oxygen species production, chemotaxis, and survival. It controls neutrophil trafficking, accumulation, and function in host defense. Thus, G-CSF negatively regulating CXCR2 signaling indicates a novel mechanism by which neutrophil recruitment and function are regulated by G-CSF in innate immunity.

In summary, our results provide evidence that, although commonly used to increase granulocyte production in the BM and to promote their mobilization, G-CSF has a negative effect on CXCR2-mediated neutrophil mobilization from the BM at a very early phase of acute inflammation. By negatively regulating CXCR2-elicited signaling, G-CSF also suppresses neutrophil activation and function. This study reveals a novel cellular mechanism for regulating neutrophil homeostasis and function during acute infection and inflammation. Neutrophils are involved in numerous pathological conditions, many of which result from homeostatic imbalance. Our findings may lead to new therapeutic strategies for the treatment of a variety of hematological, infectious, and inflammatory diseases.

MATERIALS AND METHODS

Mice

C57BL/6J mice were purchased from Charles River or The Jackson Laboratory. Mice expressing eGFP (eGFP loxP/loxP) and myeloid-specific Cre (LysM-Cre) mice were purchased from The Jackson Laboratory. eGFP gene expression was achieved by breeding eGFP mice with myeloid-specific Cre mice. All mice were housed in pathogen-free conditions at the Children's Hospital Animal Facility. 8–12-wk-old mice were used in all experiments. All procedures involving mice were monitored and approved by the Children's Hospital Animal Care and Use Committee.

Mouse peritonitis model

10^6 CFU *E. coli* (strain 19138; American Type Culture Collection) in 1 ml PBS was i.p. injected in C57BL/6J mice. At the indicated time after *E. coli* administration, the mice were euthanized by CO_2 inhalation. PB was collected by retroorbital bleeding at each time point. Neutrophil counts in the PB and BM after *E. coli* administration were measured using a hematology system (HemaVet 850; Erba Diagnostics, Inc.). Cells in the peritoneum were recovered by flushing the peritoneum cavity with 5 ml of ice-cold PBS containing 5 mM EDTA and collecting the peritoneal lavage. The process was repeated three times. To check the neutrophil content in the lungs after peritonitis, mice were euthanized by CO_2 at the indicated time after *E. coli* administration. The chest cavity was opened, and a catheter was tied to the trachea. The BAL (1 ml PBS/15 mM EDTA, 10×) was collected from each mouse in each group. The BALF was centrifuged at 450 *g* for 10 min, and the total and differential cell counts were determined from the pelleted cell fraction. The total cell counts were determined using a hemocytometer, and the differential cell counts were conducted by microscopic analysis of Wright–Giemsa-stained cytospin or with a flow cytometer (FACSCanto II) and FACSDiva software (BD). The absolute number of neutrophils was then determined based on the cytospin or FACS analysis. For microscopic analysis, neutrophils were recognized by their lobular or segmented nuclei. The percentage of polymorphonuclear neutrophils (PMNs) in the whole population (%PMN) was determined accordingly. The total number of neutrophils (#PMN) recruited was calculated as follows: #PMN = cell density × volume × %PMN. For flow cytometry analysis (Fig. S1), cells were passed through a strainer and stained with Gr1-APC (BioLegend) and CD11b-FITC (BioLegend) antibodies. Unstained cells were used as a negative control to establish the flow cytometer voltage setting, and single-color positive controls were used for adjustment of the compensation. Samples were run on a flow cytometer (FACSCanto II; BD) and analyzed using FlowJo software (Tree Star). Neutrophils were defined as Gr1$^+$CD11b$^+$ cells.

2012

Negative regulation of CXCR2 signaling by G-CSF | Bajrami et al.

MP-IVM

Mice were anesthetized with 100 mg/kg ketamine hydrochloride and 10 mg/kg xylazine i.p. The frontoparietal skull bone was exposed and prepared for IVM following previously established protocols (Mazo et al., 1998). Two-photon microscopy on the calvarium BM was performed using a fluorescence microscope (BX50WI; Olympus) equipped with a 20×, 0.95 numerical aperture objective (Olympus) and a multiphoton microscopy system (Radiance 2000MP; Bio-Rad Laboratories) controlled by Lasersharp software (Bio-Rad Laboratories). For two-photon excitation and second harmonic generation, a MaiTai Ti:Sapphire laser was tuned to a range of wavelengths from 800 to 875 nm. Mice were cannulated before imaging. Blood vessels were labeled with tetramethylrhodamine-dextran (2,000,000 MW; Invitrogen; Thermo Fisher Scientific). Neutrophils were detected by eGFP fluorescence, and bone was visualized by its second harmonic generation signal. Images were recorded every 30–40 s for 70 min after injection of MIP-2, G-CSF, indicated antibodies, or PBS. The generated image stack sequences were transformed into volume-rendered four-dimensional videos using Volocity software (PerkinElmer), which was also used for tracking cell motility in three dimensions. Directionality (0 to 1) was calculated as the straight-line migration distance from the origin divided by the total migration length. Upward directionality (−1 to 1) was calculated as the straight-line distance migrated in the direction toward the blood vessel divided by total migration length.

Immunofluorescent staining

LyzM-eGFP mice were perfused postmortem with 10 ml paraformaldehyde-lysine-periodate fixative through the vena cava to achieve rapid in situ fixation and optimal preservation of the BM tissue. Femoral bones were isolated, fixed in paraformaldehyde-lysine-periodate for 4–8 h, rehydrated in 30% sucrose/PBS for 48 h, and snap frozen in optimal cutting temperature compound (TissueTek). Cryosections of nondecalcified whole longitudinal femoral bones were obtained using a cryostat (CM3050S; Leica Biosystems) and the Cryojane tape transfer system (Leica Biosystems). After blocking with normal serum, the slides were incubated with primary antibody (rabbit anti-Ly6G from Abcam) for 30 min at room temperature. Next, the slides were washed three times with PBS followed by incubation with Texas red–conjugated goat anti–rabbit IgG secondary antibody (Thermo Fisher Scientific). DAPI (Invitrogen) staining was used for nuclear detection, and sections were mounted with Vectashield mounting medium for immunofluorescence (Vector Laboratories). High-resolution images of whole longitudinal immunostained femoral sections were obtained with an iCys Research Imaging cytometer (Compucyte Corporation) equipped with four laser lines (405, 488, 561, and 633 nm) and four photomultiplier tube detectors with bandpass emission filters at 450/40, 521/15, 575/50, and 650LP.

Cytokine/chemokine stimulation

1 µg MIP-2 in 100 µl PBS, 2 µg of human recombinant G-CSF (Neupogen; Amgen) in 100 µl of PBS, or a cocktail of both (1 µg MIP-2 and 2 µg G-CSF in 100 µl of PBS) were i.v. injected into mice. Control animals were i.v. injected with an equivalent volume of endotoxin-free PBS. Circulating neutrophil numbers were determined by collecting 50 µl PB by retroorbital puncture at the indicated time points. Blood content analysis was performed using the hematology system (HemaVet 850). The same amount of MIP-2 or G-CSF was i.v. injected into animals for intravital imaging.

Neutrophil isolation

Mouse BM-derived neutrophils were isolated using negative depletion of other cell populations using a neutrophil isolation kit (MidiMACS) following a protocol provided by the manufacturer (Miltenyi Biotec). The isolation procedure was conducted at 4°C unless specified. In brief, BM cells were filtered through a 70-µm cell strainer and suspended in 250 µl PBS containing 0.5% endotoxin-free BSA and 2 mM EDTA (magnetic-activated cell-sorting [MACS] buffer). Cells were incubated with anti–mouse Ter119, B220, CD5, CD117, CD49b, F4/80, CD4, and CD11c antibodies for 5 min, washed once with 1.5 ml of cold MACS buffer, and then incubated with goat anti–rat IgG microbeads for 5–10 min, washed with 1.5 ml MACS buffer, and suspended in 250 µl MACS buffer. Cells were subsequently loaded onto a MACS buffer–equilibrated LD column (Miltenyi Biotec) and washed twice with 1 ml MACS buffer. The flow through was harvested, washed twice with 10 ml of ice-cold RPMI medium containing 10% FBS/1% penicillin/streptomycin and allowed to warm up to room temperature in 10 ml RPMI medium until used. Human neutrophils were isolated from discarded white blood cell filters (WBF2 filter; Pall Corporation) as previously described (Zhu et al., 2006). In brief, erythrocytes were sedimented by adding an equal volume of dextran/saline solution (3% dextran T-500 in 0.9% NaCl) at room temperature for 25 min. The erythrocyte-depleted supernatants were then layered on lymphocyte separation medium (1.077 g/ml Ficoll–Hypaque solution; Voigt Global Distribution LLC) and centrifuged at 400 g at room temperature for 20 min. Contaminated erythrocytes in the neutrophil pellets were lysed after a brief (<30 s) treatment with 0.2% NaCl. Neutrophils were then resuspended in RPMI 1640 medium containing 10% heat-inactivated FBS at a density of 4×10^6 cells/ml and maintained at 37°C. The purity of neutrophils was >97% as determined by Wright–Giemsa staining. All blood was drawn from healthy blood donors. All protocols have been approved by the Children's Hospital Institutional Review Board and are subjected to annual review.

Measurement of cell signaling in mouse neutrophils

Mouse BM neutrophils were isolated by negative selection as described in the previous paragraph. Isolated BM neutro-

phils were resuspended in HBSS/0.1% BSA and treated with 0.1 µg/ml MIP-2, 0.1 µg/ml G-CSF, 0.5 µg/ml MIP-2 + G-CSF, or 0.5 µg/ml MIP-2 + G-CSF + INCB01842 for the times indicated. Cell lysates were analyzed for phosphorylated STAT3, ERK1/2, and AKT using specific antibodies (Cell Signaling Technology) by Western blotting. Actin was used as a loading control.

LPS–induced acute lung inflammation
Mice were anesthetized with 100 mg/kg ketamine hydrochloride i.p. and 10 mg/kg xylazine i.p. After anesthesia, mouse tracheas were surgically exposed (Li et al., 2009, 2011), and a total volume of 50 µl LPS (from *E. coli* o55:B5; Sigma-Aldrich) per mouse was instilled intratracheally via an angiocatheter that was inserted through the trachea and into the left bronchus. To indicate correct deposition, 1% colloidal carbon was included in the instillate. Upon completion of the experiment, mice were euthanized by CO_2.

Effect of G-CSF on neutrophil count in peritonitis model
Mice were i.v. injected with either monoclonal anti–mouse G-CSF antibody (100 µg in 100 µl PBS; R&D Systems) or human recombinant G-CSF (2 µg in 100 µl PBS; Neupogen; Amgen) 1 h before the peritoneal *E. coli* infection. Control antibody (rat anti–mouse IgG_1 antibody) or PBS was used in control experiments. Peritoneum lavage and BALF content were then analyzed.

EZ–TAXIScan chemotaxis assay
The EZ–TAXIScan chamber (Effector Cell Institute) was assembled with a 260-µm–wide × 4-µm–thick silicon chip on a 2-mm untreated glass base as described by the manufacturer and filled with RPMI medium/0.1% BSA. 1 µl of freshly purified WT mouse neutrophils (3×10^6/ml) were added to the lower reservoir of each of the six channels and allowed to line up by removing 18 µl of buffer from the upper reservoir. RPMI medium/0.1% BSA was then added to fill both reservoirs to the brim. 1 µl MIP-2 (500 ng/ml), G-CSF (500 ng/ml), fMLP (1 µM for mouse neutrophils and 100 nM for human neutrophils), IL-8 (100 nM), LTB4 (100 nM), or C5a (100 nM) was then added to the upper reservoir, and neutrophil migration (at 37°C) in each of the channels was captured sequentially every 30 s for 20 min using a 10× lens. To determine the involvement of G-CSF signaling in chemotaxis, neutrophils were exposed to 1 µg/ml G-CSF or 0.5 µg/ml JAK inhibitor INCB018424.

Analysis of cell tracks and morphology
(x,y) coordinates of migrating neutrophils (i.e., neutrophils that cross >65 µm from the starting line) were tracked from sequential images using Dynamic Image Analysis System software (Solltech). Cell tracks were then realigned such that all the cells started from the same starting point (0,0) and were plotted using Matlab (MathWorks). Chemoattractant concentration increases in the positive y direction. Directionality (0 to 1) is defined as straight-line migration distance from the origin divided by the total migration length. Upward directionality (−1 to 1) is defined as straight-line distance migrated in the upward direction divided by total migration length and migration speed. Migration speed (µm/min) was calculated as the mean of cell speeds (migration distance between the current frame and the previous frame divided by the time between sequential frames; 0.5 min) at each captured frame.

Neutrophil recruitment in the inflamed lungs
Mice were anesthetized and instilled with 50 µl LPS (from *E. coli* o55:B5; Sigma-Aldrich). At the indicated time points, mice were euthanized by CO_2. The chest cavity was opened, and a catheter was tied to the trachea. BAL was performed (1 ml PBS/15 mM EDTA 10×) in each group. The BALF was centrifuged at 450 g for 10 min, and the total and differential cell counts were determined from the pelleted cell fraction. The total number of cells in the lungs was counted by a hemocytometer. Differential cell counts were conducted on cytospin preparations stained with a modified Wright–Giemsa stain (Volu-Sol, Inc.). Neutrophils were recognized by their lobular or segmented nuclei. The percentage of pulmonary PMNs in the whole population (%PMN) was determined accordingly. Total number of pulmonary PMNs (#PMN) recruited was calculated as follows: #PMN = cell density × volume × %PMN.

BALF cytokine and chemokine levels and total protein levels
BALF samples were obtained from mice at the indicated time points. BAL was done with 1 ml of cold PBS/15 mM EDTA, flushed back and forth three times. The levels of MIP-2 and KC in the BALF were measured with ELISA kits following a protocol provided by the manufacturer (R&D Systems). Additionally a mouse 32-plex cytokine/chemokine panel was performed by Eve Technologies to evaluate the levels of cytokines and chemokines present in the lungs after intratracheal instillation of LPS or i.p. infection with *E. coli* and treatment with G-CSF antibody. Protein concentration was measured in the BALF using a protein assay reagent (Bio-Rad Laboratories). The standard curve was constructed using BSA (Su et al., 2008).

Neutrophil depletion with Gr–1 antibody
Neutrophil depletion was achieved by i.p. injection of 200 µg/kg anti-Gr1 mAb RB6-8C5. The antibody was administered i.p. to obtain a sustained depletion over the first 48 h of the experiment. Differential white blood cell count using Wright–Giemsa staining was performed to confirm that the neutrophil depletion was successful. Neutrophils were depleted by the Gr–1 antibody in both PB (∼85% depletion) and the BM (∼65% depletion; Kwak et al., 2015).

Histopathology
Lungs were collected after indicated treatment and fixed by intratracheal instillation of Bouin's solution at 23-cm H_2O pressure. Tissues were embedded in paraffin, and 6-µm–thick sections were stained with hematoxylin and eosin and examined by light microscopy. The number of neutrophils in

alveolar air spaces was quantified by morphometric analyses of histological lung sections as previously described (Mizgerd et al., 2000). ImageJ software (National Institutes of Health) was used to manually trace the neutrophil–containing regions of the tissue section and to determine the area of edema. The pixel area of each region was calculated. The neutrophil number was calculated as the total number of neutrophils outside the blood vessels in a given randomly chosen region. The edema formation was calculated as the percentage of pixel area of all the edema–containing regions relative to the pixel area of the whole image. The relative volumes of the parenchymal regions occupied by emigrated neutrophils and the level edema formation were calculated by investigators blinded to the identities of the mice.

Statistics

Results are presented as means with error bars indicating SD. Differences between groups were tested with Student's *t* test unless noted otherwise. P-values <0.05 were considered statistically significant. Neutrophil counts in PB after *E. coli* administration were analyzed by one–way ANOVA–repeated measures followed by Dunnett's multiple comparison test. Differences over time between groups were analyzed using multivariate ANOVA with measures repeated over time. Experimental group and time were the independent variables. All statistical tests and graphics were made using Prism (GraphPad Software) or SPSS Statistics software (IBM).

Online supplemental material

Fig. S1 shows flow cytometry analysis of peritoneal cells after i.p. injections of *E. coli*. Video 1 shows intravital imaging of neutrophil mobilization from the BM to circulation in an untreated mouse. Video 2 shows intravital imaging of MIP-2–induced neutrophil mobilization from the BM to circulation. Video 3 shows intravital imaging of G-CSF–induced neutrophil mobilization from the BM to circulation. Video 4 shows intravital imaging of MIP-2–induced neutrophil mobilization from the BM to circulation in a G-CSF–treated mouse. Video 5 shows chemotaxis of mouse neutrophils (untreated) in response to an MIP-2 gradient. Video 6 shows chemotaxis of G-CSF–treated mouse neutrophils in response to an MIP-2 gradient. Video 7 shows chemotaxis of mouse neutrophils in response to a G-CSF gradient. Video 8 shows chemotaxis of mouse neutrophils (untreated) in response to an fMLP gradient. Video 9 shows chemotaxis of G-CSF–treated mouse neutrophils in response to an fMLP gradient. Video 10 shows chemotaxis of mouse neutrophils treated with G-CSF and JAK inhibitor INCB018424 in response to an MIP-2 gradient. Online supplemental material is available at http://www.jem.org/cgi/content/full/jem.20160393/DC1.

ACKNOWLEDGMENTS

REFERENCES

Anderlini, P., D. Przepiorka, R. Champlin, and M. Körbling. 1996. Biologic and clinical effects of granulocyte colony-stimulating factor in normal individuals. *Blood*. 88:2819–2825.

Bardoel, B.W., E.F. Kenny, G. Sollberger, and A. Zychlinsky. 2014. The balancing act of neutrophils. *Cell Host Microbe*. 15:526–536. http://dx.doi.org/10.1016/j.chom.2014.04.011

Basu, S., A. Dunn, and A. Ward. 2002. G-CSF: function and modes of action (Review). *Int. J. Mol. Med*. 10:3–10.

Bendall, L.J., and K.F. Bradstock. 2014. G-CSF: From granulopoietic stimulant to bone marrow stem cell mobilizing agent. *Cytokine Growth Factor Rev*. 25:355–367. http://dx.doi.org/10.1016/j.cytogfr.2014.07.011

Bratton, D.L., and P.M. Henson. 2011. Neutrophil clearance: when the party is over, clean-up begins. *Trends Immunol*. 32:350–357. http://dx.doi.org/10.1016/j.it.2011.04.009

Broxmeyer, H.E. 2008. Chemokines in hematopoiesis. *Curr. Opin. Hematol*. 15:49–58. http://dx.doi.org/10.1097/MOH.0b013e3282f29012

Broxmeyer, H.E., C.M. Orschell, D.W. Clapp, G. Hangoc, S. Cooper, P.A. Plett, W.C. Liles, X. Li, B. Graham-Evans, T.B. Campbell, et al. 2005. Rapid mobilization of murine and human hematopoietic stem and progenitor cells with AMD3100, a CXCR4 antagonist. *J. Exp. Med*. 201:1307–1318. http://dx.doi.org/10.1084/jem.20041385

Burdon, P.C., C. Martin, and S.M. Rankin. 2005. The CXC chemokine MIP-2 stimulates neutrophil mobilization from the rat bone marrow in a CD49d-dependent manner. *Blood*. 105:2543–2548. http://dx.doi.org/10.1182/blood-2004-08-3193

Cheretakis, C., R. Leung, C.X. Sun, Y. Dror, and M. Glogauer. 2006. Timing of neutrophil tissue repopulation predicts restoration of innate immune protection in a murine bone marrow transplantation model. *Blood*. 108:2821–2826. http://dx.doi.org/10.1182/blood-2006-04-018184

Christopher, M.J., and D.C. Link. 2007. Regulation of neutrophil homeostasis. *Curr. Opin. Hematol*. 14:3–8. http://dx.doi.org/10.1097/00062752-200701000-00003

Chtanova, T., M. Schaeffer, S.J. Han, G.G. van Dooren, M. Nollmann, P. Herzmark, S.W. Chan, H. Satija, K. Camfield, H. Aaron, et al. 2008. Dynamics of neutrophil migration in lymph nodes during infection. *Immunity*. 29:487–496. http://dx.doi.org/10.1016/j.immuni.2008.07.012

Cornish, A.L., I.K. Campbell, B.S. McKenzie, S. Chatfield, and I.P. Wicks. 2009. G-CSF and GM-CSF as therapeutic targets in rheumatoid arthritis. *Nat. Rev. Rheumatol*. 5:554–559. http://dx.doi.org/10.1038/nrrheum.2009.178

Cottler-Fox, M.H., T. Lapidot, I. Petit, O. Kollet, J.F. DiPersio, D. Link, and S. Devine. 2003. Stem cell mobilization. *Hematology (Am Soc Hematol Educ Program)*. 2003:419–437.

Dale, D.C. 2012. Twenty years of the colony-stimulating factors. *Curr. Opin. Hematol*. 19:1–2. http://dx.doi.org/10.1097/MOH.0b013e32834e3c6e

Dale, D.C., A.A. Bolyard, M.L. Kelley, E.C. Westrup, V. Makaryan, A. Aprikyan, B. Wood, and F.J. Hsu. 2011. The CXCR4 antagonist plerixafor is a potential therapy for myelokathexis, WHIM syndrome. *Blood*. 118:4963–4966. http://dx.doi.org/10.1182/blood-2011-06-360586

Day, R.B., and D.C. Link. 2012. Regulation of neutrophil trafficking from the bone marrow. *Cell. Mol. Life Sci.* 69:1415–1423. http://dx.doi.org /10.1007/s00018-011-0870-8

DeJesus, C.E., J. Egen, M. Metzger, X. Alvarez, C.A. Combs, D. Malide, Z.X. Yu, X. Tian, and R.E. Donahue. 2011. Transient neutropenia after granulocyte-colony stimulating factor administration is associated with neutrophil accumulation in pulmonary vasculature. *Exp. Hematol.* 39:142–150. http://dx.doi.org/10.1016/j.exphem.2010.11.004

De La Luz Sierra, M., P. Gasperini, P.J. McCormick, J. Zhu, and G. Tosato. 2007. Transcription factor Gfi-1 induced by G-CSF is a negative regulator of CXCR4 in myeloid cells. *Blood.* 110:2276–2285. http://dx .doi.org/10.1182/blood-2007-03-081448

Devi, S., Y. Wang, W.K. Chew, R. Lima, N. A-González, C.N. Mattar, S.Z. Chong, A. Schlitzer, N. Bakocevic, S. Chew, et al. 2013. Neutrophil mobilization via plerixafor-mediated CXCR4 inhibition arises from lung demargination and blockade of neutrophil homing to the bone marrow. *J. Exp. Med.* 210:2321–2336. http://dx.doi.org/10.1084/jem.20130056

Doerschuk, C.M. 2000. Leukocyte trafficking in alveoli and airway passages. *Respir. Res.* 1:136–140. http://dx.doi.org/10.1186/rr24

Doerschuk, C.M., M.F. Allard, S. Lee, M.L. Brumwell, and J.C. Hogg. 1988. Effect of epinephrine on neutrophil kinetics in rabbit lungs. *J. Appl. Physiol.* 65:401–407.

Donahue, R.E., L. Tuschong, T.R. Bauer Jr., Y.Y. Yau, S.F. Leitman, and D.D. Hickstein. 2011. Leukocyte integrin activation mediates transient neutropenia after G-CSF administration. *Blood.* 118:4209–4214. http:// dx.doi.org/10.1182/blood-2011-06-360461

Eash, K.J., J.M. Means, D.W. White, and D.C. Link. 2009. CXCR4 is a key regulator of neutrophil release from the bone marrow under basal and stress granulopoiesis conditions. *Blood.* 113:4711–4719. http://dx.doi .org/10.1182/blood-2008-09-177287

Eash, K.J., A.M. Greenbaum, P.K. Gopalan, and D.C. Link. 2010. CXCR2 and CXCR4 antagonistically regulate neutrophil trafficking from murine bone marrow. *J. Clin. Invest.* 120:2423–2431. http://dx.doi.org /10.1172/JCI41649

Eyles, J.L., M.J. Hickey, M.U. Norman, B.A. Croker, A.W. Roberts, S.F. Drake, W.G. James, D. Metcalf, I.K. Campbell, and I.P. Wicks. 2008. A key role for G-CSF-induced neutrophil production and trafficking during inflammatory arthritis. *Blood.* 112:5193–5201. http://dx.doi.org/10 .1182/blood-2008-02-139535

Faust, N., F. Varas, L.M. Kelly, S. Heck, and T. Graf. 2000. Insertion of enhanced green fluorescent protein into the lysozyme gene creates mice with green fluorescent granulocytes and macrophages. *Blood.* 96:719–726.

Fibbe, W.E., J.F. Pruijt, G.A. Velders, G. Opdenakker, Y. van Kooyk, C.G. Figdor, and R. Willemze. 1999. Biology of IL-8-induced stem cell mobilization. *Ann. N.Y. Acad. Sci.* 872:71–82. http://dx.doi.org/10.1111 /j.1749-6632.1999.tb08454.x

Foxman, E.F., J.J. Campbell, and E.C. Butcher. 1997. Multistep navigation and the combinatorial control of leukocyte chemotaxis. *J. Cell Biol.* 139:1349–1360. http://dx.doi.org/10.1083/jcb.139.5.1349

Furze, R.C., and S.M. Rankin. 2008. Neutrophil mobilization and clearance in the bone marrow. *Immunology.* 125:281–288. http://dx.doi.org/10 .1111/j.1365-2567.2008.02950.x

Gordon, B.C., A.M. Revenis, A.C. Bonifacino, W.E. Sander, M.E. Metzger, A.E. Krouse, T.N. Usherson, and R.E. Donahue. 2007. Paradoxical drop in circulating neutrophil count following granulocyte–colony stimulating factor and stem cell factor administration in rhesus macaques. *Exp. Hematol.* 35:872–878. http://dx.doi.org/10.1016/j.exphem.2007 .03.011

Greenbaum, A.M., and D.C. Link. 2011. Mechanisms of G-CSF-mediated hematopoietic stem and progenitor mobilization. *Leukemia.* 25:211–217. http://dx.doi.org/10.1038/leu.2010.248

Gregory, A.D., L.A. Hogue, T.W. Ferkol, and D.C. Link. 2007. Regulation of systemic and local neutrophil responses by G-CSF during pulmonary *Pseudomonas aeruginosa* infection. *Blood.* 109:3235–3243. http://dx .doi.org/10.1182/blood-2005-01-015081

Heissig, B., K. Hattori, S. Dias, M. Friedrich, B. Ferris, N.R. Hackett, R.G. Crystal, P. Besmer, D. Lyden, M.A. Moore, et al. 2002. Recruitment of stem and progenitor cells from the bone marrow niche requires MMP-9 mediated release of kit-ligand. *Cell.* 109:625–637. http://dx.doi.org/10 .1016/S0092-8674(02)00754-7

Heit, B., S. Tavener, E. Raharjo, and P. Kubes. 2002. An intracellular signaling hierarchy determines direction of migration in opposing chemotactic gradients. *J. Cell Biol.* 159:91–102. http://dx.doi.org/10.1083/jcb .200202114

Heit, B., S.M. Robbins, C.M. Downey, Z. Guan, P. Colarusso, B.J. Miller, F.R. Jirik, and P. Kubes. 2008. PTEN functions to 'prioritize' chemotactic cues and prevent 'distraction' in migrating neutrophils. *Nat. Immunol.* 9:743–752. http://dx.doi.org/10.1038/ni.1623

Karzai, W., B.U. von Specht, C. Parent, J. Haberstroh, K. Wollersen, C. Natanson, S.M. Banks, and P.Q. Eichacker. 1999. G-CSF during *Escherichia coli* versus *Staphylococcus aureus* pneumonia in rats has fundamentally different and opposite effects. *Am. J. Respir. Crit. Care Med.* 159:1377–1382. http://dx.doi.org/10.1164/ajrccm.159.5.9806082

Kim, H.K., M. De La Luz Sierra, C.K. Williams, A.V. Gulino, and G. Tosato. 2006. G-CSF down-regulation of CXCR4 expression identified as a mechanism for mobilization of myeloid cells. *Blood.* 108:812–820. http ://dx.doi.org/10.1182/blood-2005-10-4162

Knudsen, E., P.O. Iversen, A. Bøyum, T. Seierstad, G. Nicolaysen, and H.B. Benestad. 2011. G-CSF enhances the proliferation and mobilization, but not the maturation rate, of murine myeloid cells. *Eur. J. Haematol.* 87:302–311. http://dx.doi.org/10.1111/j.1600-0609.2011.01658.x

Köhler, A., K. De Filippo, M. Hasenberg, C. van den Brandt, E. Nye, M.P. Hosking, T.E. Lane, L. Männ, R.M. Ransohoff, A.E. Hauser, et al. 2011. G-CSF-mediated thrombopoietin release triggers neutrophil motility and mobilization from bone marrow via induction of Cxcr2 ligands. *Blood.* 117:4349–4357. http://dx.doi.org/10.1182/blood-2010-09-308387

Kondo, M., A.J. Wagers, M.G. Manz, S.S. Prohaska, D.C. Scherer, G.F. Beilhack, J.A. Shizuru, and I.L. Weissman. 2003. Biology of hematopoietic stem cells and progenitors: implications for clinical application. *Annu. Rev. Immunol.* 21:759–806. http://dx.doi.org/10.1146/annurev.immunol.21 .120601.141007

Kruger, P., M. Saffarzadeh, A.N. Weber, N. Rieber, M. Radsak, H. von Bernuth, C. Benarafa, D. Roos, J. Skokowa, and D. Hartl. 2015. Neutrophils: Between host defence, immune modulation, and tissue injury. *PLoS Pathog.* 11:e1004651. http://dx.doi.org/10.1371/journal.ppat.1004651

Kwak, H.J., P. Liu, B. Bajrami, Y. Xu, S.Y. Park, C. Nombela-Arrieta, S. Mondal, Y. Sun, H. Zhu, L. Chai, et al. 2015. Myeloid cell–derived reactive oxygen species externally regulate the proliferation of myeloid progenitors in emergency granulopoiesis. *Immunity.* 42:159–171. http://dx.doi.org/10 .1016/j.immuni.2014.12.017

Leveque-El Mouttie, L., T. Vu, K.E. Lineburg, R.D. Kuns, F.O. Bagger, B.E. Teal, M. Lor, G.M. Boyle, C. Bruedigam, J.D. Mintern, et al. 2015. Autophagy is required for stem cell mobilization by G-CSF. *Blood.* 125:2933–2936. http://dx.doi.org/10.1182/blood-2014-03-562660

Levesque, J.P., F. Liu, P.J. Simmons, T. Betsuyaku, R.M. Senior, C. Pham, and D.C. Link. 2004. Characterization of hematopoietic progenitor mobilization in protease-deficient mice. *Blood.* 104:65–72. http://dx.doi .org/10.1182/blood-2003-05-1589

Lévesque, J.P., J. Hendy, Y. Takamatsu, P.J. Simmons, and L.J. Bendall. 2003. Disruption of the CXCR4/CXCL12 chemotactic interaction during hematopoietic stem cell mobilization induced by GCSF or cyclophosphamide. *J. Clin. Invest.* 111:187–196. http://dx.doi.org/10 .1172/JCI15994

2016

Negative regulation of CXCR2 signaling by G-CSF | Bajrami et al.

Li, Y., Y. Jia, M. Pichavant, F. Loison, B. Sarraj, A. Kasorn, J. You, B.E. Robson, D.T. Umetsu, J.P. Mizgerd, et al. 2009. Targeted deletion of tumor suppressor PTEN augments neutrophil function and enhances host defense in neutropenia-associated pneumonia. *Blood*. 113:4930–4941. http://dx.doi.org/10.1182/blood-2008-06-161414

Li, Y., A. Prasad, Y. Jia, S.G. Roy, F. Loison, S. Mondal, P. Kocjan, L.E. Silberstein, S. Ding, and H.R. Luo. 2011. Pretreatment with phosphatase and tensin homolog deleted on chromosome 10 (PTEN) inhibitor SF1670 augments the efficacy of granulocyte transfusion in a clinically relevant mouse model. *Blood*. 117:6702–6713. http://dx.doi.org/10.1182/blood-2010-09-309864

Liu, F., H.Y. Wu, R. Wesselschmidt, T. Kornaga, and D.C. Link. 1996. Impaired production and increased apoptosis of neutrophils in granulocyte colony-stimulating factor receptor–deficient mice. *Immunity*. 5:491–501. http://dx.doi.org/10.1016/S1074-7613(00)80504-X

Liu, L., K.D. Puri, J.M. Penninger, and P. Kubes. 2007. Leukocyte PI3Kγ and PI3Kδ have temporally distinct roles for leukocyte recruitment in vivo. *Blood*. 110:1191–1198. http://dx.doi.org/10.1182/blood-2006-11-060103

Martin, C., P.C. Burdon, G. Bridger, J.C. Gutierrez-Ramos, T.J. Williams, and S.M. Rankin. 2003. Chemokines acting via CXCR2 and CXCR4 control the release of neutrophils from the bone marrow and their return following senescence. *Immunity*. 19:583–593. http://dx.doi.org/10.1016/S1074-7613(03)00263-2

Mazo, I.B., J.C. Gutierrez-Ramos, P.S. Frenette, R.O. Hynes, D.D. Wagner, and U.H. von Andrian. 1998. Hematopoietic progenitor cell rolling in bone marrow microvessels: parallel contributions by endothelial selectins and vascular cell adhesion molecule 1. *J. Exp. Med*. 188:465–474. http://dx.doi.org/10.1084/jem.188.3.465

McColl, S.R., and I. Clark-Lewis. 1999. Inhibition of murine neutrophil recruitment in vivo by CXC chemokine receptor antagonists. *J. Immunol*. 163:2829–2835.

McDermott, D.H., Q. Liu, J. Ulrick, N. Kwatemaa, S. Anaya-O'Brien, S.R. Penzak, J.O. Filho, D.A. Priel, C. Kelly, M. Garofalo, et al. 2011. The CXCR4 antagonist plerixafor corrects panleukopenia in patients with WHIM syndrome. *Blood*. 118:4957–4962. http://dx.doi.org/10.1182/blood-2011-07-368084

McDermott, D.H., Q. Liu, D. Velez, L. Lopez, S. Anaya-O'Brien, J. Ulrick, N. Kwatemaa, J. Starling, T.A. Fleisher, D.A. Priel, et al. 2014. A phase 1 clinical trial of long-term, low-dose treatment of WHIM syndrome with the CXCR4 antagonist plerixafor. *Blood*. 123:2308–2316. http://dx.doi.org/10.1182/blood-2013-09-527226

Mei, J., Y. Liu, N. Dai, C. Hoffmann, K.M. Hudock, P. Zhang, S.H. Guttentag, J.K. Kolls, P.M. Oliver, F.D. Bushman, and G.S. Worthen. 2012. Cxcr2 and Cxcl5 regulate the IL-17/G-CSF axis and neutrophil homeostasis in mice. *J. Clin. Invest*. 122:974–986. http://dx.doi.org/10.1172/JCI60588

Metcalf, D., L. Robb, A.R. Dunn, S. Mifsud, and L. Di Rago. 1996. Role of granulocyte-macrophage colony-stimulating factor and granulocyte colony-stimulating factor in the development of an acute neutrophil inflammatory response in mice. *Blood*. 88:3755–3764.

Mizgerd, J.P., J.J. Peschon, and C.M. Doerschuk. 2000. Roles of tumor necrosis factor receptor signaling during murine *Escherichia coli* pneumonia. *Am. J. Respir. Cell Mol. Biol*. 22:85–91. http://dx.doi.org/10.1165/ajrcmb.22.1.3733

Nagase, H., M. Miyamasu, M. Yamaguchi, M. Imanishi, N.H. Tsuno, K. Matsushima, K. Yamamoto, Y. Morita, and K. Hirai. 2002. Cytokine-mediated regulation of CXCR4 expression in human neutrophils. *J. Leukoc. Biol*. 71:711–717.

Nauseef, W.M., and N. Borregaard. 2014. Neutrophils at work. *Nat. Immunol*. 15:602–611. http://dx.doi.org/10.1038/ni.2921

Pelus, L.M., and S. Fukuda. 2006. Peripheral blood stem cell mobilization: the CXCR2 ligand GRO*β* rapidly mobilizes hematopoietic stem cells with enhanced engraftment properties. *Exp. Hematol*. 34:1010–1020. http://dx.doi.org/10.1016/j.exphem.2006.04.004

Pelus, L.M., H. Bian, A.G. King, and S. Fukuda. 2004. Neutrophil-derived MMP-9 mediates synergistic mobilization of hematopoietic stem and progenitor cells by the combination of G-CSF and the chemokines GROβ/CXCL2 and GROβ$_T$/CXCL2$_{\Delta4}$. *Blood*. 103:110–119. http://dx.doi.org/10.1182/blood-2003-04-1115

Peters, N.C., J.G. Egen, N. Secundino, A. Debrabant, N. Kimblin, S. Kamhawi, P. Lawyer, M.P. Fay, R.N. Germain, and D. Sacks. 2008. In vivo imaging reveals an essential role for neutrophils in leishmaniasis transmitted by sand flies. *Science*. 321:970–974. http://dx.doi.org/10.1126/science.1159194

Petit, I., M. Szyper-Kravitz, A. Nagler, M. Lahav, A. Peled, L. Habler, T. Ponomaryov, R.S. Taichman, F. Arenzana-Seisdedos, N. Fujii, et al. 2002. G-CSF induces stem cell mobilization by decreasing bone marrow SDF-1 and up-regulating CXCR4. *Nat. Immunol*. 3:687–694. http://dx.doi.org/10.1038/ni813

Petty, J.M., C.C. Lenox, D.J. Weiss, M.E. Poynter, and B.T. Suratt. 2009. Crosstalk between CXCR4/stromal derived factor-1 and VLA-4/VCAM-1 pathways regulates neutrophil retention in the bone marrow. *J. Immunol*. 182:604–612. http://dx.doi.org/10.4049/jimmunol.182.1.604

Poon, I.K., C.D. Lucas, A.G. Rossi, and K.S. Ravichandran. 2014. Apoptotic cell clearance: basic biology and therapeutic potential. *Nat. Rev. Immunol*. 14:166–180. http://dx.doi.org/10.1038/nri3607

Sadik, C.D., N.D. Kim, and A.D. Luster. 2011. Neutrophils cascading their way to inflammation. *Trends Immunol*. 32:452–460. http://dx.doi.org/10.1016/j.it.2011.06.008

Semerad, C.L., F. Liu, A.D. Gregory, K. Stumpf, and D.C. Link. 2002. G-CSF is an essential regulator of neutrophil trafficking from the bone marrow to the blood. *Immunity*. 17:413–423. http://dx.doi.org/10.1016/S1074-7613(02)00424-7

Semerad, C.L., M.J. Christopher, F. Liu, B. Short, P.J. Simmons, I. Winkler, J.P. Levesque, J. Chappel, F.P. Ross, and D.C. Link. 2005. G-CSF potently inhibits osteoblast activity and CXCL12 mRNA expression in the bone marrow. *Blood*. 106:3020–3027. http://dx.doi.org/10.1182/blood-2004-01-0272

Smith, E., A. Zarbock, M.A. Stark, T.L. Burcin, A.C. Bruce, P. Foley, and K. Ley. 2007. IL-23 is required for neutrophil homeostasis in normal and neutrophilic mice. *J. Immunol*. 179:8274–8279. http://dx.doi.org/10.4049/jimmunol.179.12.8274

Stark, M.A., Y. Huo, T.L. Burcin, M.A. Morris, T.S. Olson, and K. Ley. 2005. Phagocytosis of apoptotic neutrophils regulates granulopoiesis via IL-23 and IL-17. *Immunity*. 22:285–294. http://dx.doi.org/10.1016/j.immuni.2005.01.011

Strydom, N., and S.M. Rankin. 2013. Regulation of circulating neutrophil numbers under homeostasis and in disease. *J. Innate Immun*. 5:304–314. http://dx.doi.org/10.1159/000350282

Su, X., M. Johansen, M.R. Looney, E.J. Brown, and M.A. Matthay. 2008. CD47 deficiency protects mice from lipopolysaccharide-induced acute lung injury and *Escherichia coli* pneumonia. *J. Immunol*. 180:6947–6953. http://dx.doi.org/10.4049/jimmunol.180.10.6947

Subramanian, K.K., Y. Jia, D. Zhu, B.T. Simms, H. Jo, H. Hattori, J. You, J.P. Mizgerd, and H.R. Luo. 2007. Tumor suppressor PTEN is a physiologic suppressor of chemoattractant-mediated neutrophil functions. *Blood*. 109:4028–4037. http://dx.doi.org/10.1182/blood-2006-10-055319

Suratt, B.T., J.M. Petty, S.K. Young, K.C. Malcolm, J.G. Lieber, J.A. Nick, J.A. Gonzalo, P.M. Henson, and G.S. Worthen. 2004. Role of the CXCR4/SDF-1 chemokine axis in circulating neutrophil homeostasis. *Blood*. 104:565–571. http://dx.doi.org/10.1182/blood-2003-10-3638

Vlahos, R., S. Bozinovski, S.P. Chan, S. Ivanov, A. Lindén, J.A. Hamilton, and G.P. Anderson. 2010. Neutralizing granulocyte/macrophage colony-stimulating factor inhibits cigarette smoke-induced lung inflammation. *Am. J. Respir. Crit. Care Med.* 182:34–40. http://dx.doi.org/10.1164/rccm.200912-1794OC

von Vietinghoff, S., and K. Ley. 2008. Homeostatic regulation of blood neutrophil counts. *J. Immunol.* 181:5183–5188. http://dx.doi.org/10.4049/jimmunol.181.8.5183

Wengner, A.M., S.C. Pitchford, R.C. Furze, and S.M. Rankin. 2008. The coordinated action of G-CSF and ELR + CXC chemokines in neutrophil mobilization during acute inflammation. *Blood.* 111:42–49. http://dx.doi.org/10.1182/blood-2007-07-099648

Zhu, D., H. Hattori, H. Jo, Y. Jia, K.K. Subramanian, F. Loison, J. You, Y. Le, M. Honczarenko, L. Silberstein, and H.R. Luo. 2006. Deactivation of phosphatidylinositol 3,4,5-trisphosphate/Akt signaling mediates neutrophil spontaneous death. *Proc. Natl. Acad. Sci. USA.* 103:14836–14841. http://dx.doi.org/10.1073/pnas.0605722103